

A seasonal analysis of aerosol NO_3^- sources and NO_x oxidation pathways in the Southern Ocean marine boundary layer

Jessica M. Burger¹, Emily Joyce², Meredith G. Hastings², Kurt A. M. Spence¹, Katye E. Altieri¹

¹Department of Oceanography, University of Cape Town, Rondebosch, 7701, South Africa

²Department of Earth, Environmental and Planetary Sciences and Institute at Brown for Environment and Society, Brown University, Providence, RI, 02906, USA.

Correspondence to: Jessica M. Burger (brgjes006@uct.ac.za)

Abstract. Nitrogen oxides, collectively referred to as NO_x ($\text{NO} + \text{NO}_2$), are an important component of atmospheric chemistry involved in the production and destruction of various oxidants that contribute to the oxidative capacity of the troposphere. The primary sink for NO_x is atmospheric nitrate, which has an influence on climate and the biogeochemical cycling of reactive nitrogen. NO_x sources and NO_x to NO_3^- formation pathways remain poorly constrained in the remote marine boundary layer of the Southern Ocean (SO), particularly outside of the more frequently sampled summer months. This study presents seasonally resolved measurements of the isotopic composition ($\delta^{15}\text{N}$, $\delta^{18}\text{O}$ and $\Delta^{17}\text{O}$) of atmospheric nitrate in coarse mode ($> 1\mu\text{m}$) aerosols, collected between South Africa and the sea ice edge in summer, winter and spring. Similar latitudinal trends in $\delta^{15}\text{N}\text{-NO}_3^-$ were observed in summer and spring, suggesting similar NO_x sources. Based on $\delta^{15}\text{N}\text{-NO}_3^-$, the dominating primary/main NO_x sources were likely a combination of lightning, biomass burning and/or soil emissions at the low latitudes, as well as oceanic alkyl nitrates and snowpack emissions from continental Antarctica or the sea ice at the low-, mid and high latitudes, respectively. Snowpack emissions associated with photolysis were derived from both the Antarctic snowpack as well as from snow on sea ice. A combination of natural NO_x sources, likely transported from the lower latitude Atlantic contribute to the background level NO_3^- observed in winter, with the potential for a stratospheric NO_{3-x}^- source evidenced by one sample of Antarctic origin. Greater values of $\delta^{18}\text{O}\text{-NO}_3^-$ in spring and winter compared to summer, suggest an increased influence of oxidation pathways that incorporate oxygen atoms from O_3 into the end product NO_3^- (i.e., N_2O_5 , DMS and ~~X~~halogen oxides (XO)) Low summertime $\delta^{18}\text{O}\text{-NO}_3^-$ ($< -70\%$) are consistent with daytime processes involving oxidation by OH dominating nitrate formation, while higher winter and springtime $\delta^{18}\text{O}\text{-NO}_3^-$ ($> -60\%$) indicate an increased influence of O_3 oxidation (i.e., N_2O_5 , DMS, BrO). Significant linear relationships between $\delta^{18}\text{O}$ and $\Delta^{17}\text{O}$ suggest isotopic mixing between $\text{H}_2\text{O}_{(\text{v})}$ and O_3 in winter, and isotopic mixing between $\text{H}_2\text{O}_{(\text{v})}$ and O_3/XO in spring with the addition of a third endmember (atmospheric O_2) becoming relevant in spring. The onset of sunlight in spring, coupled with large sea ice extent, can activate chlorine chemistry with the potential to increase peroxy radical concentrations, contributing to oxidant chemistry in the marine boundary layer.

1 Introduction

The atmosphere of the Southern Ocean is geographically remote from major anthropogenic influences. Although there is evidence of microplastics and at times long-range transport of anthropogenic pollution (Jacobi et al., 2000; Obbard 2018;), the Southern Ocean marine boundary layer (MBL) is one of the few regions dominated by natural sources, and as such at times it can serve as a proxy for the pre-industrial atmosphere. The pre-industrial

atmosphere is used as a baseline for comparing the magnitude of anthropogenic impacts on climate (e.g., Haywood and Boucher, 2000; Hamilton et al., 2014; Schmale et al., 2019).

Nitrogen oxides ($\text{NO}_x = \text{NO} + \text{NO}_2$) are an important part of biogeochemical cycling and influence the oxidative capacity of the troposphere as they are involved in the production and destruction of ozone and hydroxyl radicals (Lawrence and Crutzen, 1999; Finlayson-Pitts and Pitts, 2000). The primary sink for NO_x is atmospheric nitrate (NO_3^-), which impacts both air quality and climate by influencing particulate matter load and Earth's radiative heat budget (IPCC, 2013; (Park and Kim, 2005)).

The logistical difficulties of measurement campaigns to the remote Southern Ocean, particularly in winter, have resulted in a lack of observational data from this region including that of NO_x sources and sinks (Paton-Walsh et al., 2022). Consequently, the seasonality of NO_x cycling remains poorly constrained in the Southern Ocean MBL. Globally, fossil fuel combustion is the primary NO_x source (van der A et al., 2008), far exceeding natural emissions like biomass burning (Finlayson-Pitts and Pitts, 2000), soil processes (Davidson and Kinglerlee, 1997) and lightning (Schumann and Huntrieser, 2007). However, regional budgets of NO_x sources can have a variety of anthropogenic and natural contributors. In the summertime Southern Ocean MBL, natural NO_x sources are the mainprimary contributors to atmospheric NO_3^- formation (Morin et al., 2009; Burger et al., 2022). Along the South African coastline, these natural NO_x sources include a combination of lightning, biomass burning and soil emissions (Morin et al., 2009). In coastal Antarctica, or near to the marginal ice zone, NO_x emitted from snow cover serves as the mainprimary precursor to atmospheric NO_3^- (Savarino et al., 2007; Morin et al., 2009; Shi et al., 2021; Burger et al., 2022). Over the mid-latitude region of the Southern Ocean, sea surface emissions of a group of nitrogen gases referred to as alkyl nitrates (RONO_2), have recently been proposed as a NO_x source leading to NO_3^- formation in the MBL (Fisher et al., 2018; Burger et al., 2022). During winter, NO_x sources to the Antarctic troposphere primarily include long-range transported peroxyacetyl nitrates (PAN) and stratospheric inputs (Savarino et al., 2007; Lee et al., 2014; Walters et al., 2019). To our knowledge, however, there are no observational data regarding NO_x sources from the Southern Ocean MBL during winter, and few observations in spring.

In addition to there being multiple NO_x sources across the Southern Ocean MBL, several different oxidation pathways can be responsible for NO_x to NO_3^- conversion, varying with chemistry and time of day (Savarino et al., 2007). Once emitted, NO is rapidly oxidised by ozone (O_3) (R1), peroxy radicals (RO_2 or HO_2) (R2), and/or halogen oxides (XO ; where $\text{X} = \text{Br}, \text{Cl}, \text{or I}$) (R3), to NO_2 .



Under sunlit conditions, NO_2 is readily photolyzed to regenerate NO and O_3 (R4). The recycling of NO_x between NO and NO_2 happens much faster than NO_x oxidation to NO_3^- during the day (Michalski et al., 2003). On a global scale, NO is primarily oxidised to NO_2 by ozone (O_3), followed by although over the open ocean oxidation

74 by peroxy radicals (HO_2 and RO_2 , while NO to NO_2 oxidation via XO is relatively minor) can also occur
75 (Alexander et al., 2020).

76 During summer in the Southern Ocean MBL, NO_2 is subsequently oxidised primarily by hydroxyl radicals (OH)
77 to form HNO_3 (R5).

78 $\text{NO}_2 + \text{OH} + \text{M} \rightarrow \text{HNO}_3 + \text{M}$ (R5)

79 In winter, under dark conditions, when the photolytic production of OH stops, NO_2 is oxidised primarily by O_3 to
80 form nitrate radicals (NO_3) (R6). NO_3 can then react with NO_2 to form dinitrogen pentoxide (N_2O_5) followed by
81 hydrolysis on a wet particle surface to form HNO_3 (R7-R8).

82 $\text{NO}_2 + \text{O}_3 \rightarrow \text{NO}_3 + \text{O}_2$ (R6)

83 $\text{NO}_3 + \text{NO}_2 + \text{M} \rightleftharpoons \text{N}_2\text{O}_5(\text{g}) + \text{M}$ (R7)

84 $\text{N}_2\text{O}_5(\text{g}) + \text{H}_2\text{O}(\text{l}) + \text{surface} \rightarrow 2\text{HNO}_3(\text{aq})$ (R8)

85 Alternatively, HNO_3 can be formed by the reaction of NO_3 with hydrocarbons (HC) (e.g., dimethylsulphide
86 (DMS)) (R9).

87 $\text{NO}_3 + \text{HC or DMS} \rightarrow \text{HNO}_3 + \text{products}$ (R9)

88 Lastly, halogen in places with elevated halogen concentrations, NO_2 can be oxidised by reactive halogens (e.g.,
89 bromine oxide (BrO)), to form HNO_3 ; chemistry may result in NO_3^- formation via the production and subsequent
90 hydrolysis of halogen nitrates (R10-R11), as has been suggested for coastal Antarctica in summer (Baugitte et al.,
91 2012).

92 $\text{XO} + \text{NO}_2 \rightarrow \text{XNO}_3$ (R10)

93 $\text{XNO}_3 + \text{H}_2\text{O}(\text{l}) + \text{surface} \rightarrow \text{HNO}_3(\text{aq}) + \text{HOX}$ (R11)

94 The nitrogen (N) and oxygen (O) isotopic composition of atmospheric NO_3^- provides information regarding NO_x
95 sources and NO_3^- formation pathways (i.e., NO oxidation to NO_2 and NO_2 oxidation to NO_3^-). This technique has
96 been applied in polluted (Elliot et al., 2007; Zong et al., 2017), open ocean (Hastings et al., 2003; Altieri et al.,
97 2013; Kamezaki et al., 2019; Burger et al., 2022) and polar environments (Walters et al., 2019). Stable isotope
98 ratios are reported as the ratio of the heavy to light isotopologues of a sample relative to the constant isotopic ratio
99 of a reference standard, using delta (δ) notation in units of “per mil” (‰) following Eq. (1):

100
$$\delta = \left(\left(R_{\text{sample}} / R_{\text{standard}} \right) - 1 \right) \times 1000 \quad (1)$$

101 where R represents the ratio of $^{15}\text{N}/^{14}\text{N}$, $^{18}\text{O}/^{16}\text{O}$ or $^{17}\text{O}/^{16}\text{O}$ in the sample and in the reference standard,
102 respectively. The reference for O is Vienna Standard Mean Ocean Water (VSMOW) and for N is atmospheric N_2
103 (Bolhke et al., 2003).

104 The N isotopic composition of atmospheric NO_3^- ($\delta^{15}\text{N}-\text{NO}_3^-$) largely reflects the $\delta^{15}\text{N}$ of different precursor NO_x
105 emissions (e.g., Elliott et al., 2019 and references therein), but can be influenced by isotopic fractionation during

Formatted: Subscript

Formatted: Subscript

Formatted: Subscript

Formatted: Subscript

Formatted: Subscript

Formatted: Subscript

NO_x cycling and NO_x to NO₃⁻ conversion (Walters and Michalski 2015; Walters et al., 2016; Li et al., 2021). δ¹⁵N-NO₃⁻ is therefore useful for constraining NO_x sources. For example, ~~the δ¹⁵N of lightning NO_x is approximately 0‰ (Hoering, 1957); biomass burning may produce NO_x with a δ¹⁵N range of -7 to 12‰ (Fibiger and Hastings, 2016), while soils lead to NO_x emissions with relatively low δ¹⁵N signatures (-44.2 to -14.0‰; Miller et al., 2018). More relevant to the remote Southern Ocean is lightning NO_x which has a δ¹⁵N signature of approximately 0‰ (Hoering, 1957). This~~ and is distinct from the snowpack NO_x source, which typically has a very low δ¹⁵N signature ~~of ~-48‰ (Berhanu et al., 2014; Berhanu et al., 2015) on the order of -50 to -20‰ (Wagenbach et al., 1998; Winton et al., 2020); depending on the degree of snowpack NO₃⁻ ¹⁵N enrichment (Shi et al., 2018).~~ Savarino et al., (2007) derived an Antarctic stratospheric NO_x source signature of 19 ± 3‰. Additionally, Burger et al. (2022) estimated the δ¹⁵N signature of NO_x produced by surface ocean RONO₂ emissions over the mid-latitude Southern Ocean to be ~~~ 21.8 ± 2.6‰.~~

The O isotopic composition of atmospheric NO₃⁻ (δ¹⁸O- and Δ¹⁷O-NO₃⁻) reflects the oxidants responsible for NO₃⁻ formation, as atmospheric oxidants have distinct O isotope signatures (Michalski et al., 2011). δ¹⁸O-NO₃⁻ and Δ¹⁷O-NO₃⁻ are thus useful for identifying pathways of NO₃⁻ production (Michalski et al., 2003; Hastings et al., 2003; Alexander et al., 2020). O₃ possesses a distinctively large ¹⁷O excess as a result of non-mass-dependent isotope fractionation. This ¹⁷O excess is expressed as Δ¹⁷O = δ¹⁷O - 0.52 x δ¹⁸O (Berhanu et al., 2012). Non-mass dependent fractionation occurs in the troposphere and is ~~thought to originate from related to asymmetric molecules of excited ozone (O₃^{*}) that lose excess energy via stabilisation to product O₃ UV-photolysis breaking oxygen molecules to form O₃ (Heidenreich & Thiemens, 1986; Ireland et al., 2020).~~ As a result, O₃ possesses a uniquely high terminal Δ¹⁷O = 39.2 ± 2‰ (Vicars and Savarino, 2014) that can be transferred to NO₃⁻ during oxidation reactions between NO_x and O₃ (Thiemens 2006; ~~Savarino et al., 2008; Michalski and Bhattacharya, 2009), or NO_x and other oxidants like XO where the oxygen atom originated from O₃ (Savarino et al., 2016).~~ Δ¹⁷O-NO₃⁻ therefore ~~can~~ serves as a proxy for the influence of O₃ ~~and/or XO~~ during NO₃⁻ formation (Berhanu et al., 2012).

O₃ also has a uniquely high terminal δ¹⁸O = 126.3 ± 11.9‰ (Vicars and Savarino, 2014) compared to other oxidants that have a Δ¹⁷O of 0‰ and much lower δ¹⁸O signatures (Michalski et al., 2003; Michalski et al., 2011). For example, atmospheric O₂ has a δ¹⁸O signature of 23.9‰ and the δ¹⁸O of OH and H₂O are negative (Michalski et al., 2011). As such, a higher δ¹⁸O or Δ¹⁷O for atmospheric NO₃⁻ reflects the increased influence of O₃ ~~and/or XO~~ on NO₃⁻ formation, while a lower δ¹⁸O or Δ¹⁷O occurs when there is ~~an increased contribution from other oxidants lack of exchange of O atoms with O₃~~ (Hastings et al., 2003; Fang et al., 2011; Altieri et al., 2013). Oxidation by peroxy radicals would also result in a lower δ¹⁸O and Δ¹⁷O signature for atmospheric nitrate because the O atom in peroxy radicals derives from atmospheric ~~ce~~ O₂.

~~Antarctic t~~Tropospheric oxidation chemistry has been well characterised using Δ¹⁷O at coastal (Savarino et al., 2007; Ishino et al., 2017) and interior Antarctic sites (Frey et al., 2009; Savarino et al., 2016; Walters et al., 2019). A distinct seasonal cycle in Δ¹⁷O-NO₃⁻ is generally observed whereby a higher relative contribution from O₃ oxidation and/or stratospheric input occurs during winter, and more HO_x + RO_x oxidation occurs during summer. The Atlantic Southern Ocean is less constrained in terms of oxidation chemistry, with growing evidence that the atmospheric oxidant budget is poorly understood in unpolluted low-NO_x environments (Beygi et al., 2011).

143 This study presents the first seasonally resolved data set of coarse mode ($> 1 \mu\text{m}$) atmospheric NO_3^- concentration
144 and isotopic composition from the Atlantic Southern Ocean MBL. Using air mass back trajectories and observed
145 aerosol $\delta^{15}\text{N}-\text{NO}_3^-$, $\delta^{18}\text{O}-\text{NO}_3^-$ and $\Delta^{17}\text{O}-\text{NO}_3^-$ between Cape Town, South Africa and the marginal ice zone this
146 work aims to identify how the main sources and formation pathways of NO_3^- vary over the remote Southern Ocean
147 from winter through spring and summer.

148 2 Methods

149 2.1 Sample collection

150 Samples were collected on board the Research Vessel (R/V) *SA Agulhas II* during three voyages to and from the
151 marginal ice zone in summer (7th to 21st December 2018 & 27th February to 15th March 2019), winter (19th July to
152 12th August 2019) and spring (13th October to 19th November 2019) (Fig. 1). The summer samples presented here
153 are the same as those in Burger et al. (2022). The winter and spring samples were collected and analysed as in
154 Burger et al. (2022), with any methodological modifications noted below. Briefly, all voyages departed from Cape
155 Town (33.9° S, 18.4° E) and sailed southward along the Good Hope transect (0°E), until reaching Penguin Bukta
156 (71.4° S, 2.5° W) in summer and the northern extent of the sea ice in winter (approximately 58.1° S) and spring
157 (approximately 59.3° S). The ship then returned to Cape Town, sailing north via the Good Hope transect, with a
158 deviation to South Georgia in the summer. In spring an additional ice edge transect was conducted during which
159 the ship sailed from 0 to approximately 22° E and back, before returning to Cape Town.

160 Size-segregated aerosols were collected on the ninth floor above the bridge (approximately 20 m above sea level),
161 using a high-volume air sampler (HV-AS; Tisch Environmental). Air was pumped at an average flow rate of 1.3
162 $\text{m}^3 \text{min}^{-1}$ through a five-stage cascade impactor (TE-235; Tisch Environmental), loaded with pre-combusted
163 (400°C for 4 hours) glass fibre filters. Given that aerosol nitrate in the MBL is predominantly present in the coarse
164 mode ($> 1 \mu\text{m}$), only filter stages 1 through 4 were analysed. The aerodynamical diameter of particles captured
165 by filter stages 1, 2, 3 and 4 are $> 7 \mu\text{m}$, 3 to 7 μm , 1.5 to 3 μm and 1 to 1.5 μm , respectively.

166 A sector collector was used to restrict HV-AS activity to avoid contamination of the filters with ship stack
167 emissions (Campbell Scientific Africa). The HV-AS only operated if the winds were blowing at an angle less than
168 120° or greater than 240° from the bow of the ship during winter, and less than 75° or greater than 190° from the
169 bow of the ship during spring. These criteria were altered based on the dominant wind direction during each
170 voyage to ensure sufficient sample collection while avoiding contamination. In addition to wind direction, the
171 wind speed had to exceed 0 m s^{-1} for ten minutes for the HV-AS to begin sampling. Filters were removed from
172 the cascade impactor inside a laminar flow cabinet (Air Science), placed in individual zip-sealed bags and stored
173 at -20°C until analysis.

174 An attempt was made to ensure that there were at least 24 hours of in-sector sampling before removing filters
175 from the cascade impactor, to ensure atmospheric NO_3^- concentrations were sufficient for isotope analysis (Sect.
176 2.3). However, this was not always possible as on occasion filters had to be removed early due to unusual ship
177 manoeuvres that could have resulted in sample contamination by ship stack emissions if left unattended. Sampling
178 duration ranged from 11 to 36 hours in winter and 7 to 41 hours in spring (Table S1).

During each voyage, a field blank was collected by fitting the cascade impactor with a set of filters and loading the HV-AS in the same manner that atmospheric samples were deployed. The cascade impactor was then immediately removed without turning on the HV-AS pump. The field blanks were removed from the cascade impactor and stored in the same manner as the atmospheric samples. All chemical analysis performed on samples was performed on the field blanks to assess any possible contamination during filter deployment or laboratory procedures.

2.2 Sample analysis

Once back on land, filters were extracted using ultra-clean deionised water (DI; 18 MΩ) under a laminar flow cabinet (Air Science). The extraction ratio was approximately 30 cm² to 100 cm² of filter in 30 mL of DI. Extracts were immediately sonicated for one hour and then stored at 4°C for at least 12 hours. Thereafter, extracts were filtered (0.2 μm) using an acid washed syringe into clean 30 mL HDPE bottles and stored at -20°C until analysis (Burger et al., 2022).

2.2.1 NO₃⁻ concentration analysis

[NO₃⁻] was determined using a Thermo Scientific Dionex Aquion Ion Chromatography (IC) system equipped with an autosampler. The anion IC contained an AG22 RFIC 4 x 50 mm guard column and AG22 RFIC 4 x 250 mm analytical column. A six-point standard curve was run on each day of analysis (Dionex Seven Anion-II Standard) and an R² value > 0.999 was required for sample analysis to proceed. Final [NO₃⁻] were corrected by subtracting the field blanks, which represented on average 32% and 59% of the [NO₃⁻] in winter and spring, respectively. Where the field blank had a [NO₃⁻] greater than that of the sample, the sample [NO₃⁻] was assumed to be zero. Samples were measured for [NO₃⁻] only once to preserve sample volume for isotopic analysis (Sect. 2.2.2.3), motivated by the small difference between repeated sample measurements from the summertime dataset (SD_p = 0.3 μmol L⁻¹). It is important to note that given the low [NO₃⁻] of the field blanks (< 1.5 μM), no isotopic analysis could be performed using blank filters.

2.2.2.1 Isotopic analysis

The isotopic composition of atmospheric NO₃⁻ (δ¹⁵N, δ¹⁸O, and Δ¹⁷O-NO₃⁻) was measured using the denitrifier method (Sigman et al., 2001; Casciotti et al., 2002; Kaiser et al., 2007). In brief, a natural strain of denitrifying bacteria, *Pseudomonas aureofaciens*, that lack the terminal nitrous oxide (N₂O) reductase enzyme were used to convert aqueous NO₃⁻ quantitatively to N₂O gas. The product N₂O was analyzed by Gas-Chromatograph IRMS (Thermo- Scientific Delta V Plus) for simultaneous isotopic determination of ¹⁵N/¹⁴N and ¹⁸O/¹⁶O (Sigman et al., 2001; Casciotti et al., 2002). The ¹⁵N/¹⁴N of samples was corrected for the contribution of ¹⁷O to the peak at mass 45 using Δ¹⁷O determined for each sample, with values ranging from 21.7‰ to 44.4‰. International reference materials (Table S2) IAEA-N3 and USGS34 were used to normalize isotopic values to air (δ¹⁵N), and IAEA-N3, USGS34 and USGS-35 were used to normalize to VSMOW (δ¹⁸O) scales. The pooled standard deviation of sample replicates and duplicates for δ¹⁵N was 0.19‰ (n = 16) and for δ¹⁸O was 0.27‰ (n = 16). The pooled standard deviations of sample references IAEA-N3, USGS-34, USGS-35 for δ¹⁵N and for δ¹⁸O are reported for each season in Table S3.

Formatted: Font: Bold

215 For winter and spring samples, $\Delta^{17}\text{O}-\text{NO}_3^-$ was characterized by using a separate 50 nmol aliquot to convert NO_3^-
216 to N_2O , thermally decomposing the N_2O to N_2 and O_2 in a gold furnace at 770°C and analyzing the isotopic
217 composition of O_2 for determination of $^{18}\text{O}/^{16}\text{O}$ and $^{17}\text{O}/^{16}\text{O}$ (Kaiser et al., 2007; Fibiger et al., 2013). The product
218 O_2 was referenced to USGS34 and USGS35, and a 50/50 mix of USGS34 and USGS35 was also quantified within
219 runs serving as a quality control check. The pooled standard deviations for $\Delta^{17}\text{O}$ were 0.84‰ (n=21), 0.90‰
220 (n=21), and 0.61‰ (n=18) for USGS34, USGS35, and the 50/50 mix, respectively. The pooled standard deviation
221 of sample replicates and duplicates was 0.63‰ in winter and 0.31‰ in spring.

222
223 It is important to note that given the low $[\text{NO}_3^-]$ of the field blanks ($< 1.5 \mu\text{M}$), no isotopic analysis could be
224 performed on the blank filters and therefore the blank was not subtracted from the isotope results. However, we
225 note that there was no relationship found between the blank percent contribution and $\delta^{15}\text{N}-$ or $\delta^{18}\text{O}-\text{NO}_3^-$ for
226 spring and winter. This indicates that the measured signal is not driven by the blank contribution.

227 228 2.2.3 Sea water sampling and NO_2^- concentration analysis

229 Seawater samples were collected in triplicate every two hours from the ships underway system (position at depth
230 approximately 5 m) for the analysis of surface ocean nitrite concentrations ($[\text{NO}_2^-]$). Seawater samples for NO_2^-
231 determination where immediately frozen at -20°C and stored in dark conditions until analysis. $[\text{NO}_2^-]$ was analysed
232 using the colorimetric method of Grasshof et al. (1983) using a Thermo Scientific Genesys 30 visible
233 spectrophotometer (detection limit of $0.05 \mu\text{mol L}^{-1}$). The majority of seawater $[\text{NO}_2^-]$ analysis was conducted
234 while at sea.

235 **2.3 Air mass back trajectory analysis**

236 Airmass back trajectories (AMBTs) were computed for each hour in which the HV-AS was operational for at least
237 45 minutes of that hour. Given that the ship was moving, a different date, time and starting location was used to
238 compute each AMBT. An altitude of 20 m was chosen to match the height of the HV-AS above sea level and 72-
239 hour AMBTs were computed to account for the lifetime of NO_3^- in the atmosphere. Model estimates of the
240 atmospheric lifetime of NO_3^- range from approximately three to five days (Lu et al., 2021). AMBTs become
241 increasingly uncertain the further back in time they are used (Sinclair et al., 2013), particularly in the remote
242 Southern Hemisphere. To minimize this uncertainty, the shortest possible AMBTs are generated while still
243 accounting for the lifetime of NO_3^- (i.e., 72-hours). Daily 120-hour AMBTs computed for the duration of each
244 voyage were additionally computed (See supplemental), to confirm that even when utilising the maximum
245 estimate for NO_3^- atmospheric lifetime, no continental influence from southern Africa is expected. All AMBTs
246 were computed with NOAA's Hybrid Single-Particle Lagrangian Integrated Trajectory (HYSPLIT) model (Stein
247 et al., 2015; Rolph et al., 2017), using NCEP Global Data Assimilation System (GDAS) output, which can be
248 accessed at <http://www.arl.noaa.gov/ready/hysplit4.html> (NOAA Air Resources Laboratory, Silver spring,
249 Maryland).

250 **3 Results and Discussion**

Formatted: Line spacing: 1.5 lines

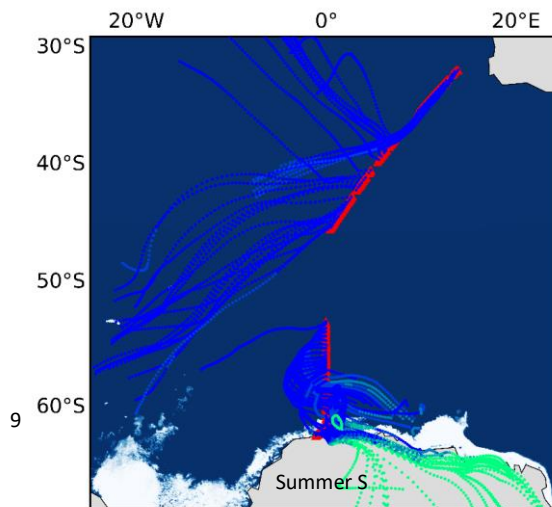
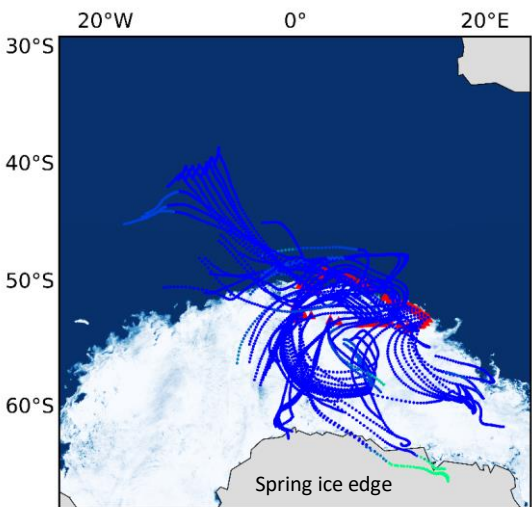
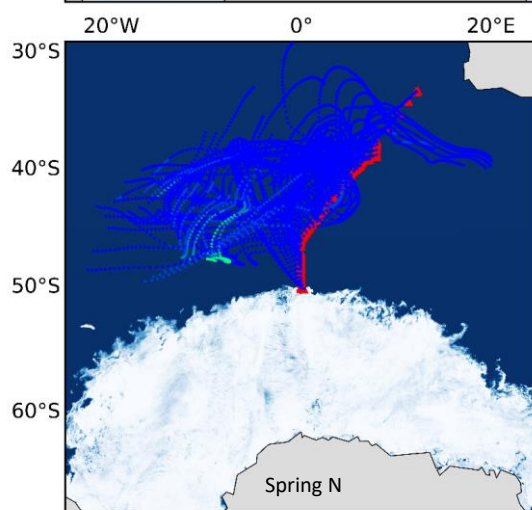
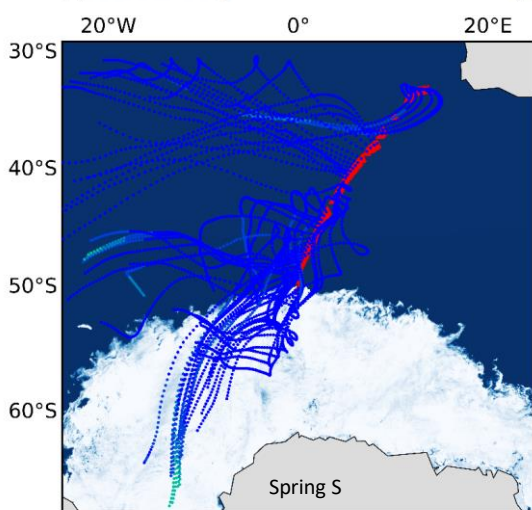
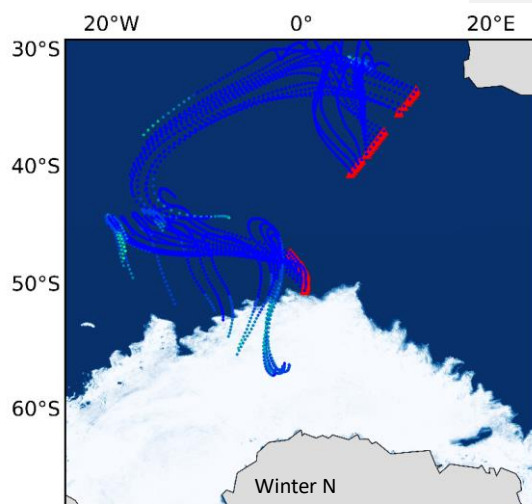
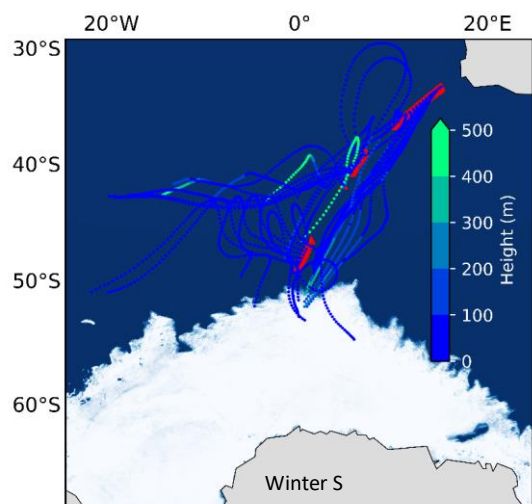
Formatted: Normal, Left, Line spacing: single

Formatted: Font: Bold

Formatted: Font: (Default) Times New Roman, Bold

Formatted: Font: Bold

~~During all three seasons sampling was conducted across the Atlantic Southern Ocean.~~ AMBTs indicate that no samples experienced any continental influence from South Africa (Fig 1), such that no direct anthropogenic emission sources are considered. 72-hour AMBTs confirm that the Atlantic sector of the Southern Ocean was a dominant source region for most samples collected throughout all seasons. Airmasses experienced very little interaction with sea ice in winter (Fig 1a & b), while extensive interaction with sea ice was experienced by airmasses sampled in spring, particularly at the high latitudes during the south bound leg (Fig 1c) and ice edge transect (Fig 1e). In summer, some high latitudes air masses traversed coastal Antarctica before being sampled, particularly on the south bound leg (Fig 1f), while some interaction with sea ice was also experienced by high latitude air masses on both legs (Fig 1f & g). The potential for sea ice influence is supported by the relatively low height (< 100 m) of AMBTs (Fig. 1). As a result, air masses originated from a mixture of source regions ranging from the open ocean to sea ice to Antarctic continental ice. The remoteness of all the locations at which air masses originated from motivates the investigation of natural NO_x sources below.



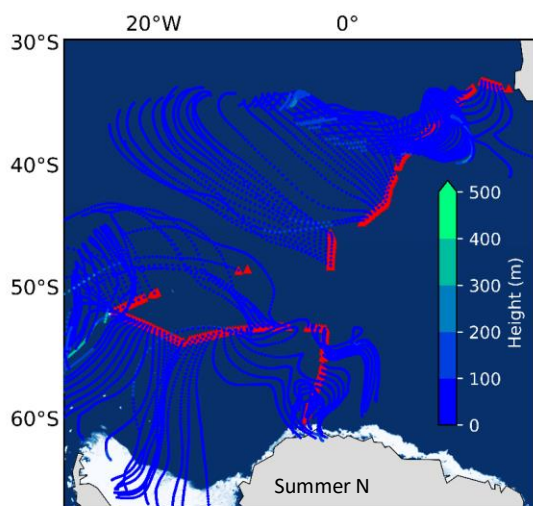
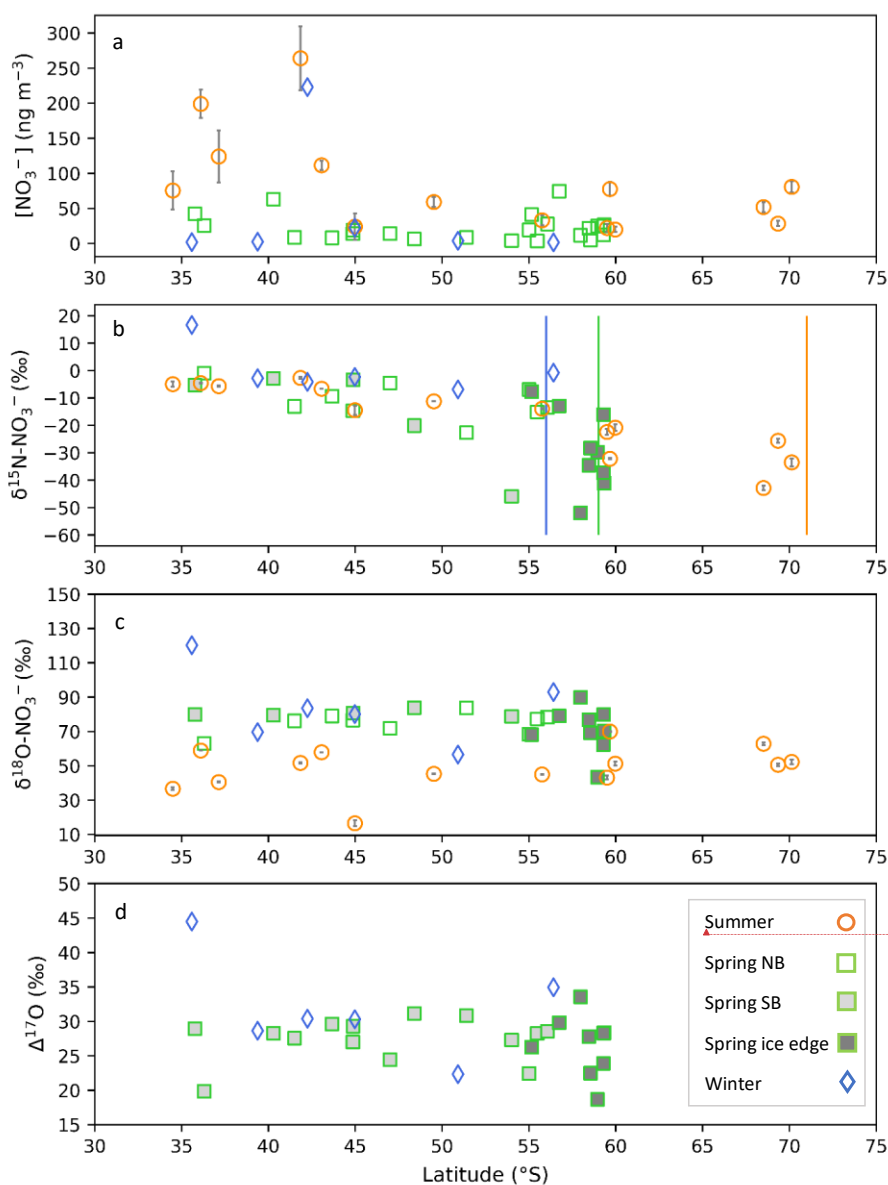


Figure 1. 72-hour AMBTs computed for each hour of every filter deployment made in winter (19th July to 12th August 2019) on both the southbound (Winter S) and northbound (Winter N) voyages, in spring (13th October to 19th November 2019) on the southbound voyage (Spring S), northbound voyage (Spring N) and ice edge transect (Spring ice edge) and in summer (7th to 21st December 2018 & 27th February to 15th March 2019) on the southbound (Summer S) and northbound (Summer N) voyages. Red triangles indicate the ships cruise track during each filter deployment. The AMBTs are coloured by height (m) (blue to green colour bar).

Figure 1. 72-hour AMBTs computed for each hour of every filter deployment (grey lines) made in winter on both the southbound (a) and northbound (b) voyages, in spring on the southbound voyage (c), ice edge transect (d) and northbound voyage (e) and in summer on the southbound (f) and northbound (g) voyages. Red circles indicate the ships cruise track during each filter deployment.

3.1 Seasonal variation in atmospheric NO_3^- concentrations

In winter, atmospheric $[\text{NO}_3^-]$ were very low across the Atlantic Southern Ocean ranging from below detection to 22.3 ng m^{-3} (Fig. 2a2; blue diamonds). A single outlier exists with a relatively high $[\text{NO}_3^-]$ equivalent to 222.9 ng m^{-3} in winter, although it is comparable to summertime $[\text{NO}_3^-]$ (Fig. 2a2; orange circles). In spring, atmospheric $[\text{NO}_3^-]$ ranged from 3.3 ng m^{-3} to 74.4 ng m^{-3} , with one sample below detection limit. Higher $[\text{NO}_3^-]$ were observed at the lower latitudes and at the higher latitudes, while lower $[\text{NO}_3^-]$ were observed in the mid-latitude Atlantic Southern Ocean (Fig. 2a2; green squares). During summer atmospheric $[\text{NO}_3^-]$ were higher than winter and spring, ranging from 19.9 ng m^{-3} to 264.0 ng m^{-3} . In contrast to winter and spring, a distinct latitudinal trend was observed in summer whereby the $[\text{NO}_3^-]$ decreased with increasing latitude (Fig. 2a2; orange circles) (Burger et al., 2022).



Formatted: Font: (Default) +Body (Calibri), 10 pt

Formatted: Font: Font color: Auto

Figure 2. The average coarse mode ($> 1 \mu m$) atmospheric nitrate concentration $[NO_3^-]$ (ng m⁻³) (a), weighted average $\delta^{15}N$ of atmospheric nitrate ($\delta^{15}N-NO_3^-$ (‰ vs. N₂)) (b), $\delta^{18}O$ of atmospheric nitrate ($\delta^{18}O-NO_3^-$ (‰ vs. VSMOW)) (c) and $\Delta^{17}O$ of atmospheric nitrate ($\Delta^{17}O-NO_3^-$ (‰)) (d) as a function of latitude (°S). Winter, spring and summer are denoted by blue diamonds, green squares, and orange circles, respectively. For the summer data,

where error bars (± 1 SD) are not visible, the standard deviation is smaller than the size of the marker. Spring data are separated into northbound (NB), southbound (SB) and ice edge legs by clear, light grey and dark grey fills, respectively for panels b-d. Vertical lines indicate the approximate location of the sea ice edge in summer (orange), winter (blue) and spring (green), identified visually using satellite derived sea ice concentration obtained from passive microwave sensors AMSR2 (Advanced Microwave Scanning Radiometer 2; Spreen et al., 2008). The average coarse mode ($> 1 \mu\text{m}$) atmospheric nitrate concentration $[\text{NO}_3^-]$ (ng m^{-3}) as a function of latitude ($^\circ\text{S}$). Winter, spring and summer are denoted by blue diamonds, green squares, and orange circles, respectively. For the summer data, where error bars (± 1 SD) are not visible, the standard deviation is smaller than the size of the marker.

The seasonal cycle in atmospheric $[\text{NO}_3^-]$ that we observe, i.e., lowest concentrations in winter, higher in spring and highest in summer, is similar to previous observations for the region. Atmospheric $[\text{NO}_3^-]$ ranging from tens of ng m^{-3} to approximately 100 ng m^{-3} have been observed for the Southern Ocean MBL during late spring (Morin et al., 2009; Shi et al., 2021) and observations from a coastal Antarctic sites in the Atlantic sector at east Antarctica showed elevated $[\text{NO}_3^-]$ (> 2040 to 70 ng m^{-3}) in throughout late spring and to early summer (Wagenbach et al., 1998; Wolff et al., 2008; Shi et al., 2022). Seasonal studies at coastal and inland Antarctic sites observed the lowest $[\text{NO}_3^-]$ during winter (Wagenbach et al., 1998; Savarino et al., 2007; Wolff et al., 2008; Ishino et al., 2017; Walters et al., 2019).

The seasonality in atmospheric $[\text{NO}_3^-]$ is largely driven by the seasonality in sunlight availability. Maximum atmospheric $[\text{NO}_3^-]$ observed in late spring/early summer in coastal Antarctica were attributed to reactive N released from the post depositional processing/recycling of snow NO_3^- (Savarino et al., 2007). After NO_3^- is deposited to the snowpack, it can be photochemically reduced to NO_x , and (re)emitted to the overlying atmosphere (Jones et al., 2000; Jones et al., 2001). During winter, extended periods of darkness lead to reduced photochemical activity above the snow, resulting in background level $[\text{NO}_3^-]$ (Lee et al., 2014). Over the open ocean, increased UV radiation in spring and summer compared to winter may lead to greater NO_3^- production from the photolytically derived oceanic RONO_2 source (Fisher et al., 2018). Ground-based studies at various Antarctic sites in Antarctica demonstrate that UV radiation is highest in spring and is highest in early summer, when stratospheric O_3 concentrations are at a minimum and the noon solar zenith angle is low (Aun et al., 2020; Lakkala et al., 2020; Li et al., 2020). This, in addition to greater lightning NO_x production during spring and summer at the lower southern latitudes ($< 40^\circ\text{S}$) (Nesbitt et al., 2000) likely explain why higher $[\text{NO}_3^-]$ are observed in spring and summer as compared to winter.

3.2 Seasonal variation in NO_x sources

While $[\text{NO}_3^-]$ provides valuable information regarding the seasonal and spatial variation in the quantity of tropospheric NO_3^- present, the N isotopic composition serves as a useful tool for identifying NO_x sources that lead to aerosol NO_3^- formation. Here, we present and interpret the mass weighted coarse-mode average $\delta^{15}\text{N}-\text{NO}_3^-$, computed for each filter deployment. In remote environments where O_3 concentrations largely exceed NO_x concentrations, as is the case for the remote Southern Ocean, NO_x isotopic exchange occurs at a much slower rate than the Leighton Cycle reactions. Therefore, little to no equilibrium isotope fractionation is expressed, and the $\delta^{15}\text{N}$ of NO_3^- is assumed to reflect the $\delta^{15}\text{N}$ of the NO_x source (Walters et al., 2016).

Formatted: Subscript

Formatted: Subscript

Formatted: Subscript

3.2.1 Evidence for stratospheric NO_3^-

There was one unusually high $\delta^{15}\text{N}-\text{NO}_3^-$ value equivalent to 16.6‰ for the first filter deployment of the southbound leg in winter. Despite an elevated $\delta^{15}\text{N}$ signature, its $[\text{NO}_3^-]$ was consistent with that of most wintertime samples. The $\delta^{15}\text{N}-\text{NO}_3^-$ of this wintertime sample is similar to the $\delta^{15}\text{N}$ of stratospherically sourced NO_3^- , estimated to be $19 \pm 3\text{‰}$ (Savarino et al., 2007). Stratospheric input is additionally supported by the air mass history of this sample, which indicates that air originated from as far south as the sea ice edge for the duration of the sample deployment (Fig. 1a). Near the sea ice edge, some AMBTs originate from greater heights (300 to 400 m) and descend towards the sampling location (< 100 m) (Fig. S1).s. Coastal Antarctic studies suggest that the deposition of PSCs during winter results in stratospheric NO_3^- inputs to the Antarctic troposphere (Wagenbach et al., 1998; Savarino et al., 2007). Winter, when this sample was collected is the only time of year when Antarctic temperatures are expected to be cold enough (< 195 K) for polar stratospheric cloud (PSC) formation (von Savigny et al., 2005; Wang et al., 2008).

Furthermore, this sample is unique in that it has a relatively high $\delta^{18}\text{O}-\text{NO}_3^-$ and $\Delta^{17}\text{O}-\text{NO}_3^-$, 120.2‰ and 44.5‰, respectively. Tropospheric oxidation typically produces $\Delta^{17}\text{O}-\text{NO}_3^-$ values ranging from 17.3‰ to 42.7‰ (Morin et al., 2011; Ishino et al., 2017; Walters et al., 2019). Stratospheric sourced $\Delta^{17}\text{O}-\text{NO}_3^-$ is elevated in comparison to tropospheric $\Delta^{17}\text{O}-\text{NO}_3^-$ because stratospheric O_3 has a greater isotope anomaly than tropospheric O_3 , and/or dominance of the N_2O_5 and ClONO_2 pathways allow for greater transfer of the anomaly to NO_3^- via O_3 (Savarino et al., 2007; McCabe et al., 2007). High $\Delta^{17}\text{O}-\text{NO}_3^-$ (> ~40‰) observed in winter, are often attributed to contributions by stratospheric denitrification (Savarino et al., 2007; McCabe et al., 2007; Frey et al., 2009; Walters et al., 2019). The combination of elevated $\Delta^{17}\text{O}-\text{NO}_3^-$ and $\delta^{15}\text{N}-\text{NO}_3^-$ is consistent with a stratospheric NO_3^- source for this sample. Given the evidence that this sample likely does not reflect tropospheric oxidation chemistry, it is left out of the below analysis.

3.2.2 Transported NO_x

Previous modelling studies suggest have shown that tropospheric transport of NO_x emitted in the from the mid to low latitudes (i.e., soil, lightning, thermal decomposition of peroxyacetylnitrate (PAN) and fossil fuel combustion), contributes to the Antarctic NO_3^- budget in winter (Lee et al., 2014; Shi et al., 2018). PAN decomposition has previously been suggested as a NO_x source to coastal Antarctica during winter and early spring (Savarino et al., 2007; Jones et al., 2011). However, transported NO_x results in minimal NO_3^- , regarded as background level concentrations (Lee et al., 2014), consistent with most of our winter observations (Fig. 2a2; blue diamonds). During winter, $\delta^{15}\text{N}-\text{NO}_3^-$ was relatively invariant across the Atlantic Southern Ocean (Fig. 2b3; blue diamonds) with an average of $-3.4 \pm 2.1\text{‰}$ ($n = 5$). This is consistent with a lack of snowpack NO_x emissions at the high latitudes during July/August due to weak or absent solar radiation (Shi et al., 2022). Furthermore, air mass back trajectory analyses indicate that sea ice had a very minor influence on the winter samples (Fig. 1a & b).

Figure 3. The weighted-average $\delta^{15}\text{N}$ of atmospheric nitrate ($\delta^{15}\text{N}-\text{NO}_3^-$ (‰ vs. N_2)) as a function of latitude (° S). Winter, spring and summer are denoted by blue diamonds, green squares, and orange circles, respectively. For the summer data, where error bars (± 1 SD) are not visible, the standard deviation is smaller than the size of the marker. Spring data are separated into northbound (NB), southbound (SB) and ice edge legs by clear, light grey and dark grey fills, respectively. Vertical lines indicate the approximate location of the sea ice edge in summer

Formatted: Subscript

(orange), winter (blue) and spring (green), identified visually using satellite derived sea ice concentration obtained from passive microwave sensors AMSR2 (Advanced Microwave Scanning Radiometer 2; Spreen et al., 2008).

Albeit outside of the winter months, previous studies report an average $\delta^{15}\text{N-NO}_3^-$ for the low latitude Atlantic Ocean (between 45°S and 45°N) on the order of -3 to -4‰ (Baker et al., 2007; Morin et al., 2009), attributed to a combination of natural NO_x sources including lightning, biomass burning and soil emissions (Morin et al., 2009). This is also similar to the spring observations where higher values of $\delta^{15}\text{N-NO}_3^-$ were observed at the lower latitudes ($-3.2 \pm 1.8\text{‰}$; $n = 3$). As such, the winter samples and low-latitude spring samples could be representative of a combination of natural NO_x sources emitted further north and transported to the mid-to-low latitude Atlantic Ocean.

Not all winter samples isotopically indicative of the transported background NO_x source had low $[\text{NO}_3^-]$. One unusually high $[\text{NO}_3^-]$ value (222.9 ng m^{-3}) was observed in at the lower latitudes (Fig. 2a2; blue diamonds). Due to the similarity in isotopic composition among winter samples, we can assume that despite a higher $[\text{NO}_3^-]$, this sample also originated from a combination of natural NO_x sources transported from the lower latitudes. Furthermore a $[\text{NO}_3^-]$ on the order of 200 ng m^{-3} is consistent with summertime $[\text{NO}_3^-]$ observations (Fig. 2a2; orange circles), when natural NO_x sources dominated (see section 3.2.3). Our results thus confirm that like in summer, natural NO_x sources can at times lead to relatively high $[\text{NO}_3^-]$, even in winter when background conditions are typically experienced.

In addition, the winter dataset presented here clearly highlights the utility of the isotopes in distinguishing NO_x sources. The initial winter sample had a low concentration indicative of the background conditions; however, the triple stable isotopic composition of the sample confirms that it originated from the stratosphere (see sect. 3.2.1). In contrast, the anomalously high $[\text{NO}_3^-]$ sample observed in winter was not consistent with minimal background NO_x emissions, however its $\delta^{15}\text{N}$ confirmed that this was in fact the most likely source.

3.2.3 Snowpack photolysis and oceanic NO_x sources

Springtime $\delta^{15}\text{N-NO}_3^-$ ranged from -52.0‰ to -1.1‰ and samples with the lowest $\delta^{15}\text{N-NO}_3^-$ were observed at the high latitudes (Fig. 2b3; green squares). The range in $\delta^{15}\text{N-NO}_3^-$ observed for spring is consistent with late spring/early summer (November to December) observations from the Indian Ocean sector of the Southern Ocean (Shi et al., 2021) and summer (December and March) observations from the Atlantic sector (Burger et al., 2022). Springtime $\delta^{15}\text{N-NO}_3^-$ is also consistent with long-term records of $\delta^{15}\text{N-NO}_3^-$ measured at coastal Antarctica (Wagenbach et al., 1998) and on the east Antarctic Plateau (Winton et al., 2020), for the same season. Given the similarity in $\delta^{15}\text{N-NO}_3^-$ between spring and summer we expect the dominant NO_x sources to be the same.

During spring, air mass back trajectories indicate substantial sea ice influence at the high latitudes during the southbound leg and during the ice edge transect (Fig. 34a & c). There is a large isotope effect associated with snow NO_3^- photolysis during summer in the Antarctic (Berhanu et al., 2014, 2015; Frey et al., 2009; Erbland et al., 2013), resulting in the emission of low $\delta^{15}\text{N-NO}_x$ ($\sim -48\text{‰}$) to the overlying atmosphere (Savarino et al., 2007; Morin et al., 2009; Shi et al., 2018; Walters et al., 2019). The low $\delta^{15}\text{N-NO}_3^-$ samples from the high latitudes (minimum -52.0‰) are clearly influenced by sea ice (Fig. 2b3, Fig. 34a & c), but the air masses do not cross the Antarctic continent. This suggests that the low $\delta^{15}\text{N-NO}_x$ likely comes from snow nitrate photolysis from the snow on sea ice, before a net loss of NO_3^- from the snowpack leads to any large ^{15}N enrichment in the snow and

Formatted: Font: Not Italic

subsequently the atmosphere (Shi et al., 2018). We conclude that NO_x as a result of photolysis of snow nitrate on sea ice can explain the relatively low $\delta^{15}\text{N}\text{-NO}_3^-$ observed in samples collected at the high latitudes on the spring southbound leg and during the ice edge transect (Fig. 2b grey filled squares).”

This suggests that the low $\delta^{15}\text{N}\text{-NO}_x$ likely comes from snow nitrate photolysis from the snow on sea ice. We conclude that NO_3^- photolysis from snow on sea ice can explain the relatively low $\delta^{15}\text{N}\text{-NO}_3^-$ observed in samples collected at the high latitudes on the spring southbound leg and during the ice edge transect (Fig. 3 grey filled squares).

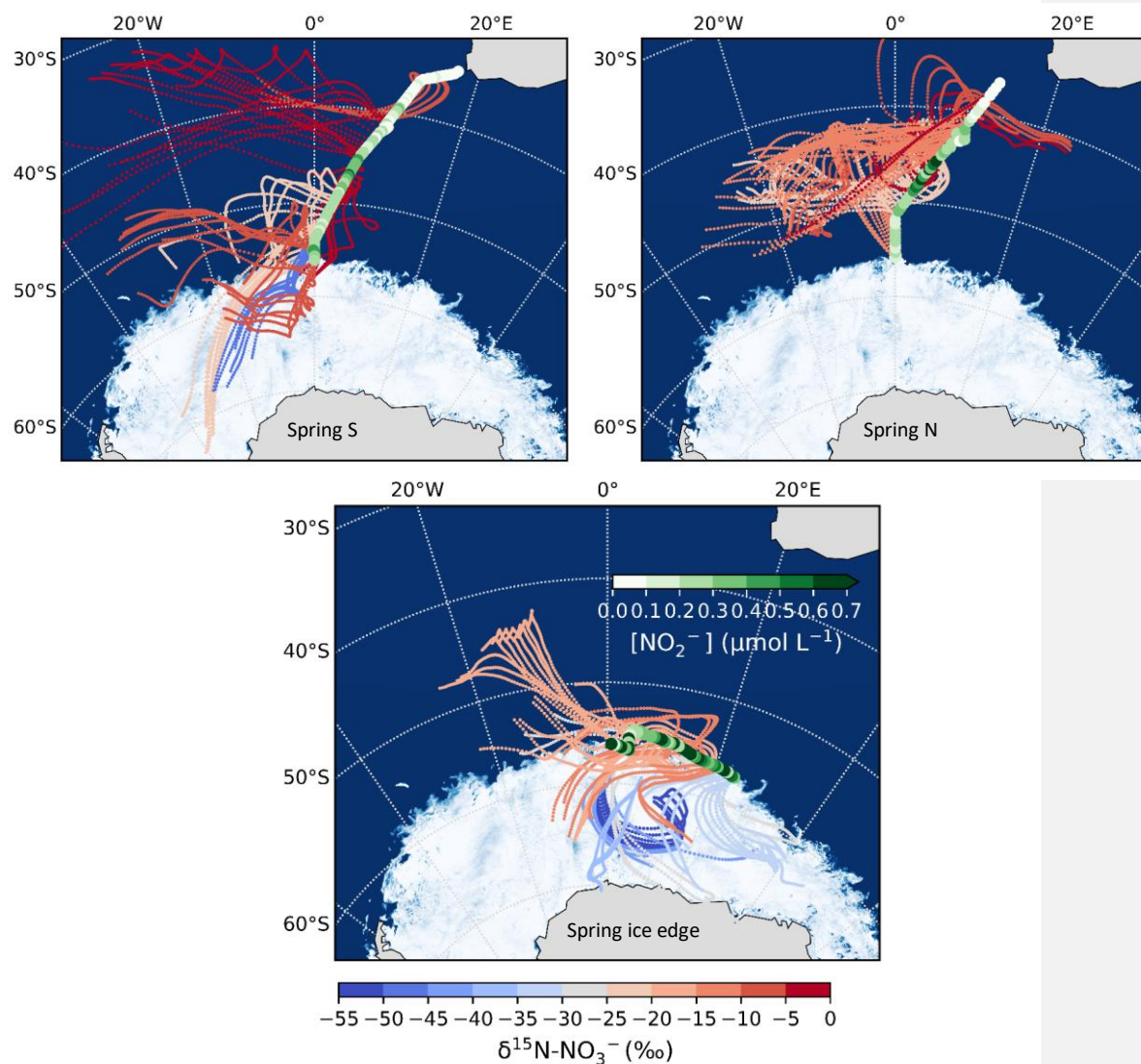


Figure 34. 72-hour AMBTs computed for each hour of the spring cruise during the southbound leg (Spring Sa), the northbound leg (Spring Nb) and the ice edge transect (Spring ice edge), when the HV-AS was running for more than 45 min of the hour. AMBTs are colour coded by the weighted average $\delta^{15}\text{N-NO}_3^-$, represented by the blue to red colour bar. Overlaid are the surface ocean nitrite concentrations ($[\text{NO}_2^-]$), represented by the green colour bar. The white area represents the location of the sea ice determined using satellite-derived sea ice concentration data obtained from the passive microwave sensors ASMR2 (Advanced Microwave Scanning Radiometer2; Spreen et al., 2008).

Higher $\delta^{15}\text{N-NO}_3^-$ values (-22.7 to -1.0‰) were observed during spring for the northbound leg (Fig. 2b open squares; Fig. 3b). The $\delta^{15}\text{N}$ of atmospheric NO_3^- that originates from snowpack emissions, depends on the $\delta^{15}\text{N}$ of the local snowpack NO_x source. ^{15}N enrichment in the snow due to preferential loss of ^{14}N during photolysis- NO_2^- loss, can eventually lead to increased $\delta^{15}\text{N-NO}_3^-$ via photolysis, and ultimately higher values of atmospheric $\delta^{15}\text{N-NO}_3^-$ (Shi et al., 2018). However, the air mass histories of the samples with air mass histories that indicate no contact with surrounding sea ice (i.e., the northbound leg; Fig. 2b3 open squares; Fig. 34b), suggesting that limited any influence from snowpack NO_x emissions was limited. These samples originated from over the mid-latitude region of the Southern Ocean where detectable sea surface nitrite was present (Fig. 34b). The NO which originates from derived from seawater nitrite in seawater is thought to limit sea surface RONO_2 production. As a result, such that non-zero elevated nitrite concentrations are required for RONO_2 production to occur in seawater (Dahl & Saltzman 2008; Dahl et al., 2012). Oceanic RONO_2 has been long proposed as an important primary NO_x source to the Antarctic (Jones et al., 1991). Recent studies have used modelling and isotopic approaches to investigate the relative importance of oceanic RONO_2 compared to other sources of NO_3^- in the Southern Ocean MBL, particularly in summer recently been proposed as an important NO_3^- source to the region in summer (Fisher et al., 2018; Burger et al., 2022). However, limited co-occurring ocean atmosphere measurements are available to constrain the seasonality of the RONO_2 source. While $\delta^{15}\text{N-RONO}_2$ has yet to be directly quantified, it was recently estimated to have an average $\delta^{15}\text{N}$ signature of ~ -22‰ in the summertime Southern Ocean (Burger et al., 2022) and -27.8‰ in the eastern equatorial Pacific (Joyce et al., 2022). Consistent with this relatively isotopically light oceanic RONO_2 source are observations of relatively low aerosol $\delta^{15}\text{N-NO}_3^-$ from the mid-latitude Southern Ocean (Burger et al., 2022) and eastern equatorial Pacific (Kamezaki et al., 2019; Joyce et al., 2022), on the order of -15 to -7‰.

Trends in $\delta^{15}\text{N-NO}_3^-$ by air mass origin were most evident in the ice edge transect during which lower (higher) $\delta^{15}\text{N-NO}_3^-$ values were observed for samples with greater sea ice (oceanic) influence (Fig. 34c). The photolysis imprint on the NO_3^- stable isotope signal in the marine boundary layer above the sea ice is clearly observed and speaks to the importance of snow-covered sea ice as a NO_x source in the region during spring as well as summer. The increased importance of oceanic RONO_2 emissions as air mass origin migrates from sea ice covered to open ocean zones is also evidenced by the decrease in $\delta^{15}\text{N-NO}_3^-$ observed for air mass originating predominantly from over the ocean (Fig. 34c).

Isotopically, there is little evidence of RONO_2 emissions contributing to aerosol NO_3^- in the winter samples. Reduced levels of UV radiation and minimal daylight hours (Fig. S24) in winter likely hinders the contribution of the oceanic NO_x source to NO_3^- loading compared to spring/summer, despite detectable sea surface nitrite concentrations in winter (Fig. S32). Additionally, photolysis in spring/summer serves to produce OH which is the primary oxidant for conversion of RONO_2 -derived NO_x in the MBL (Fisher et al., 2018).

Some studies suggest that the photolysis of particulate NO_3^- (p- NO_3^-) associated with sea-salt aerosols in the MBL can serve as an important NO_x source (Zhou et al., 2003; Ye et al., 2016; Reed et al., 2017). However, the importance of this NO_x formation pathway remains unclear, with large variability in reported rates between studies (Ye et al., 2016; Reed et al., 2017; Kasibhatla et al., 2018; Romer et al., 2018). To our knowledge, there are no observations of p- NO_3^- photolysis from the Southern Ocean MBL, and the implications of this process on the isotopic composition of NO_3^- in the MBL have yet to be assessed. We know that NO_3^- photolysis in snow is

Formatted: Superscript

Formatted: Superscript

Formatted: Font: Italic

Formatted: Not Highlight

Formatted: Not Highlight

Formatted: Not Highlight

Formatted: Not Highlight

Formatted: Not Highlight

Formatted: Not Highlight

Formatted: Subscript

Formatted: Superscript

associated with a large fractionation, leading to the emission of isotopically light NO_x while the remaining NO_3^- pool becomes enriched in ^{15}N (eg., Frey et al., 2009; Berhanu et al., 2014; 2015; Shi et al., 2018). Thus, if the NO_3^- we measured was affected by photolysis we would have expected to observe much higher or even positive values of $\delta^{15}\text{N}-\text{NO}_3^-$ during spring and summer. Another scenario is that the p-NO_3^- we measured resulted from the oxidation of NO_x released by prior p-NO_3^- photolysis. In this case, we would have expected to observe much lower $\delta^{15}\text{N}-\text{NO}_3^-$ values over the open ocean, on par with those observed over the ice. Since neither of the above scenarios matches the observations, we discount the potential influence of aerosol NO_3^- photolysis as a significant NO_x source to the region during our study is unlikely.

Additionally, a strong anti-correlation ($r = -0.86$) is observed between $\delta^{15}\text{N}-\text{NO}_3^-$ and $\Delta^{17}\text{O}-\text{NO}_3^-$ for samples collected in spring which experience a greater than 75% sea ice influence (Fig. 4), determined based on air mass history. A similar relationship was observed at Dome C during summer (Erbland et al., 2013; Savarino et al., 2016). Previous studies found that the production of enhanced $\Delta^{17}\text{O}-\text{NO}_3^-$ in polar regions is linked to the intensity of NO_x emissions from the snowpack (Moring et al., 2012; Savarino et al., 2016). The correlation between $\Delta^{17}\text{O}-\text{NO}_3^-$ and $\delta^{15}\text{N}-\text{NO}_3^-$ could arise from an increased contribution of HONO photolysis to total OH production, which is co-emitted with NO_x from the snowpack (Grannas et al., 2007), and induces a greater ^{17}O excess in OH compared to the OH production pathway: $\text{O}(\text{D}) + \text{H}_2\text{O}$ (Savarino et al., 2016). It could also arise from the coupling of snowpack emissions with reactive halogen chemistry as suggested by Morin et al. (2012). The $\Delta^{17}\text{O}/\delta^{15}\text{N}$ relationship presented here for the spring samples with air mass histories that indicate extensive influence from snow covered sea ice, suggests that snowpack emissions may lead to enhanced $\Delta^{17}\text{O}$ transfer to NO_3^- .

Formatted: Font: (Default) Times New Roman, 10 pt

Formatted: Font: (Default) Times New Roman, 10 pt, Font color: Auto

Formatted: Font color: Auto

Formatted: Font: (Default) Times New Roman, 10 pt, Font color: Auto

Formatted: Font color: Auto

Formatted: Font: (Default) Times New Roman, 10 pt, Font color: Auto

Formatted: Font: (Default) Times New Roman, 10 pt

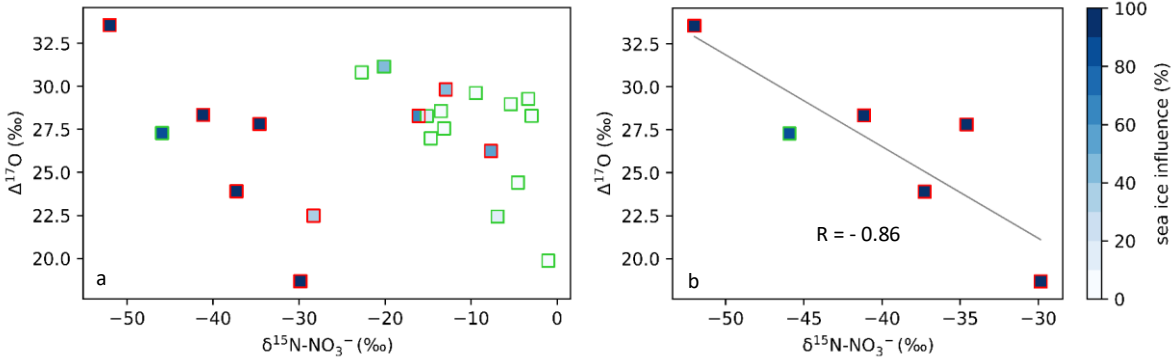


Figure 4. The relationship between $\Delta^{17}\text{O}-\text{NO}_3^-$ and $\delta^{15}\text{N}-\text{NO}_3^-$ in spring (square symbols). In both panels, samples collected along the ice edge are denoted by the red edge colour, with all other samples collect on the north and southbound legs of the voyage denoted by the green edge colour. The colour bar (blues) indicates the percentage sea influence experienced by each filter sample as determined using AMBTs. In panel a, all spring samples are included. In panel b, only samples that experienced a sea ice influence > 75% are included. A straight line (grey) is fitted to the data in panel b. Note the difference in x axis scale between panels.

3.3 Seasonal variation in oxidation

As mentioned in Sect. 1.1, the oxidation of NO and NO₂ can be determined using the oxygen isotopic composition of aerosol NO₃⁻. Here, we present and interpret the mass weighted coarse-mode average δ¹⁸O-NO₃⁻ and Δ¹⁷O-NO₃⁻, computed for each filter deployment.

During NO and NO₂ oxidation, the oxygen atoms of the responsible oxidants are incorporated into the NO₃⁻ product. The transferrable terminal oxygen atom of O₃ possesses an elevated Δ¹⁷O-NO₃⁻(O_{3term}) and δ¹⁸O(O_{3term}) (39.3 ± 2‰ and 126.3 ± 11.9‰, respectively) (Vicars & Savarino, 2014), compared to other oxidants (e.g., OH and peroxy radicals (RO₂/HO₂)) which possess a Δ¹⁷O-NO₃⁻ ≈ 0‰ (Michalski et al., 2011). The δ¹⁸O of OH is negative while the δ¹⁸O of RO₂/HO₂ stems from that of atmospheric O₂ which is also low (23.9‰; Barkan and Luz 2005). These differences allow us to ~~qualitatively~~ qualitatively assess NO and NO₂ oxidation chemistry involving contributions by various oxidants. Similarly to previous work conducted in the Southern Ocean MBL and in Antarctica (Walters et al., 2019; Shi et al., 2021), we make the assumption as prior work suggests that oxidant δ¹⁸O values are known and directly represented in the NO₃⁻.

The relatively low δ¹⁸O-NO₃⁻ values observed in summer (< 70‰; Fig. 2c5) are consistent with NO₂ oxidation via OH (Burger et al., 2022). During summer, unusually low δ¹⁸O-NO₃⁻ values were also observed equating to less than the minimum expected for the OH oxidation pathway (< ~46‰; Burger et al., 2022). This was attributed to an increased contribution by HO₂/RO₂ during NO oxidation to NO₂ (as opposed to O₃) which would decrease the δ¹⁸O of the product NO₃⁻. Increased abundance of RO₂ in the MBL was attributed to RONO₂ photolysis, hypothesized to occur over the mid latitude Southern Ocean (Fisher et al., 2018; Burger et al., 2022), and/or the presence of sea ice, which can lead to enhanced peroxy radical production (Brough et al., 2019).

~~Figure 5. The weighted average δ¹⁸O of atmospheric nitrate (δ¹⁸O-NO₃⁻ (‰ vs. VSMOW)) as a function of latitude (° S). Winter, spring and summer are denoted by blue diamonds, green squares, and orange circles, respectively. Spring data are separated into northbound (NB), southbound (SB) and ice edge legs by clear, light grey and dark grey fills, respectively. For the summer data, where error bars (± 1 SD) are not visible, the standard deviation is smaller than the size of the marker.~~

Interestingly, despite NO_x sources being the same in spring and summer (sect. 3.2), the δ¹⁸O-NO₃⁻ data suggest that the NO₃⁻ formation pathways differ (Fig. 2c5). Higher average δ¹⁸O-NO₃⁻ values were observed in spring compared to summer (Fig. 2c5). Higher δ¹⁸O-NO₃⁻ values in spring compared to summer may originate from NO_x oxidation by XO. In the Antarctic boundary layer, enhanced levels of BrO occur in spring, over sea ice covered areas (Theys et al., 2011). The production of inorganic bromine has been proposed to be related to frost flowers on thin sea ice (Kaleschke et al., 2004) and blowing of saline snow on sea ice (Yang et al., 2010). Significant interaction with sea ice cover was experienced in spring, particularly at the ice edge transect, which could have promoted NO₃⁻ formation via the BrO pathway, resulting in increased values of δ¹⁸O-NO₃⁻.

~~T~~Indeed, the oxygen isotopic composition of NO₃⁻ in winter and spring were comparable as indicated by both δ¹⁸O (Fig. 2c5) and Δ¹⁷O (Fig. 2dS3). The δ¹⁸O-NO₃⁻ ranged from 56.5‰ to 92.9‰ in winter (Fig. 2c5; blue diamonds) and from 62.3‰ to 89.8‰ in spring (Fig. 2c5; green squares). The Δ¹⁷O-NO₃⁻ ranged from 22.3‰ to 35‰ in winter (Fig. 2dS3; blue diamonds) and from 18.7‰ to 33.6‰ in spring (Fig. 2dS3; green squares).

524 Interestingly, there is more variability in the $\delta^{18}\text{O}$ and $\Delta^{17}\text{O}$ for the ice edge transect (Fig. 2c5 & 2d53; dark shaded
 525 squares) than the north and southbound transects. The overlap in $\delta^{18}\text{O}$ and $\Delta^{17}\text{O}$ in winter and spring suggest that
 526 similar pathways lead to NO_3^- formation in both seasons, i.e., oxidation pathways that result in an increased
 527 influence of O_3 during oxidation (i.e., N_2O_5 , DMS, XO).
 528 A significant linear relationship was observed between $\delta^{18}\text{O}\text{-NO}_3^-$ and $\Delta^{17}\text{O}\text{-NO}_3^-$ in both winter and spring (Fig.
 529 S4). This suggests isotopic mixing between two major oxidants (e.g., Fibiger et al., 2013; Shi et al., 2021). As
 530 such, the highest end-member is representative of tropospheric O_3 , and/or XO with a $\delta^{18}\text{O}$ of ~114 to 138‰ and
 531 a $\Delta^{17}\text{O}$ of ~39‰. There are multiple options for the second oxidant with a $\Delta^{17}\text{O} = 0\text{‰}$, i.e., water vapour ($\text{H}_2\text{O}_{(\text{v})}$),
 532 OH, and O_2 . Here, we use the $\delta^{18}\text{O}\text{-H}_2\text{O}_{(\text{v})}$ from the average of observations along a similar cruise transect from
 533 the Indian sector of the Southern Ocean (Dar et al., 2020). The average $\delta^{18}\text{O}\text{-H}_2\text{O}_{(\text{v})}$ determined between ~33° S
 534 and ~60° S ($-13.9 \pm 1.4\text{‰}$) was used for the winter samples given that AMBTs indicate that most air masses
 535 originated within this latitudinal band, where there is minimal variation in $\delta^{18}\text{O}\text{-H}_2\text{O}_{(\text{v})}$ (Dar et al., 2020). In
 536 spring, the zone of air mass origin for our samples extends further south to ~70° S. As shown by Dar et al. (2020),
 537 $\delta^{18}\text{O}\text{-H}_2\text{O}_{(\text{v})}$ declines significantly between ~60° S and ~70° S. To account for this lowering in $\delta^{18}\text{O}\text{-H}_2\text{O}_{(\text{v})}$ which
 538 could influence higher latitude samples, an additional $\text{H}_2\text{O}_{(\text{v})}$ end member equivalent to the minimum observed
 539 by Dar et al., 2020 (-27.5‰) was included for spring. The $\delta^{18}\text{O}\text{-OH}$ was calculated from the equilibrium
 540 fractionation between OH and $\text{H}_2\text{O}_{(\text{v})}$ (Walters & Michalski et al., 2016) using the observed atmospheric
 541 temperature range for winter and spring. The $\delta^{18}\text{O}\text{-OH}$ determined for winter ranges from -56.2 to -49.5‰
 542 (average = -52.8‰) and for spring ranges from -54.5 to -50.5‰ (average = -52.5‰). Therefore, a value of -53.2‰
 543 was used for both seasons. The atmospheric $\delta^{18}\text{O}\text{-O}_2$ is well-constrained at 23.9‰ (Barkan and Luz 2005). The
 544 $\delta^{18}\text{O}$ and $\Delta^{17}\text{O}$ values assumed for all oxidants or oxygen sources outlined above, are summarised in Table 1.
 545 Mixing lines for the three oxidant pairs (OH/ O_3 , $\text{H}_2\text{O}_{(\text{v})}$ / O_3 and O_2/O_3) are indicated by the grey, orange and red
 546 lines, respectively in Figure 6.

547 Table 1: A summary of the oxygen isotope ratios ($\delta^{18}\text{O}$ and $\Delta^{17}\text{O}$) for the end member oxidants and/or oxidant
 548 sources (O_3 , OH, HO_2/RO_2 and H_2O) utilised in Sect. 3.3.

Oxidant/source	$\delta^{18}\text{O}$ (‰)	References	$\Delta^{17}\text{O}$ (‰)	References
Terminal O_3	126.3 ± 11.9	Vicars & Savarino (2014)	39.3 ± 2	Vicars & Savarino (2014)
OH	-52.7 ± 2.8^a	Walters & Michalski (2016)	~0	Michalski et al. (2011)
HO_2/RO_2	23.88 ± 0.03	Barkan & Luz (2005)	~0	Michalski et al. (2011)
H_2O	-13.9 ± 1.4	Dar et al. (2020)	~0	Michalski et al. (2011)

549 ^aThe average $\delta^{18}\text{O}\text{-OH}$ was calculated from the equilibrium fractionation between OH and $\text{H}_2\text{O}_{(\text{v})}$ (Walters &
 550 Michalski, 2016) using the observed atmospheric temperature range for winter and spring and the average $\delta^{18}\text{O}\text{-}$
 551 H_2O (Dar et al., 2020).

552 To determine the lower endmember in each season, i.e., the second major oxidant in addition to ozone and/or XO,
 553 a straight line was fitted to the data in $\delta^{18}\text{O}\text{-}\Delta^{17}\text{O}$ space and the x-intercept at a $\Delta^{17}\text{O} = 0\text{‰}$ was determined. The
 554 x-intercept in winter is ~16‰. During winter, the linear relationship observed (Fig. 56a) is similar to what has
 555 been seen in the Indian Ocean MBL and at coastal east Antarctica, where the x intercept was $-11 \pm 8\text{‰}$ (Shi et al.,
 556 2021) and $-15 \pm 6\text{‰}$ (Shi et al., 2022), respectively. The oxygen isotopic composition of the lower end member
 557 in our winter data is most similar to that of $\text{H}_2\text{O}_{(\text{v})}$. This is consistent with the average $\delta^{18}\text{O}\text{-H}_2\text{O}_{(\text{v})}$ ($= -13.96 \pm$

Formatted: Not Highlight

Formatted: Font: (Default) Times New Roman, 10 pt

Formatted: Font: (Default) Times New Roman, 10 pt

Formatted: Font: (Default) Times New Roman, 10 pt, Font color: Auto

Formatted: Font: (Default) Times New Roman, 10 pt, Font color: Auto

Formatted: Font: 10 pt, Font color: Auto

Formatted: Font: (Default) Times New Roman, 10 pt, Font color: Auto

Formatted: Font: 10 pt, Font color: Auto

Formatted: Font: (Default) Times New Roman, 10 pt, Font color: Auto

Formatted: Font: (Default) Times New Roman, 10 pt, Font color: Auto

Formatted: Font: 10 pt, Font color: Auto

Formatted: Font: (Default) Times New Roman, 10 pt, Font color: Auto

Formatted: Font: 10 pt, Font color: Auto

Formatted: Font: (Default) Times New Roman, 10 pt, Font color: Auto

Formatted: Font: (Default) Times New Roman, 10 pt, Font color: Auto

Formatted: Font: 10 pt, Font color: Auto

Formatted: Font: (Default) Times New Roman, 10 pt, Font color: Auto

Formatted: Font: 10 pt, Font color: Auto

Formatted: Font: (Default) Times New Roman, 10 pt, Font color: Auto

Formatted: Font: (Default) Times New Roman, 10 pt, Font color: Auto

Formatted: Font: 10 pt, Font color: Auto

Formatted: Font: (Default) Times New Roman, 10 pt, Font color: Auto

Formatted: Font: 10 pt, Font color: Auto

Formatted: Font: (Default) Times New Roman, 10 pt, Font color: Auto

Formatted: Font: (Default) Times New Roman, 10 pt, Font color: Auto

Formatted: Left, Line spacing: Multiple 1.08 li

1.45‰) observed between approximately 33° S and 60° S (Dar et al., 2020). Therefore, a mixing line between $\text{H}_2\text{O}_{(\text{v})}$ and O_3 is the best fit to the winter observations (Fig. 56a; solid orange line). If we exclude an equilibrium isotope fractionation between OH and $\text{H}_2\text{O}_{(\text{v})}$ (Michalski et al., 2011) such that $\delta^{18}\text{O}\text{-OH}$ is similar to the $\delta^{18}\text{O}$ of $\text{H}_2\text{O}_{(\text{v})}$, then the lower end-member likely results from the OH oxidation pathway.

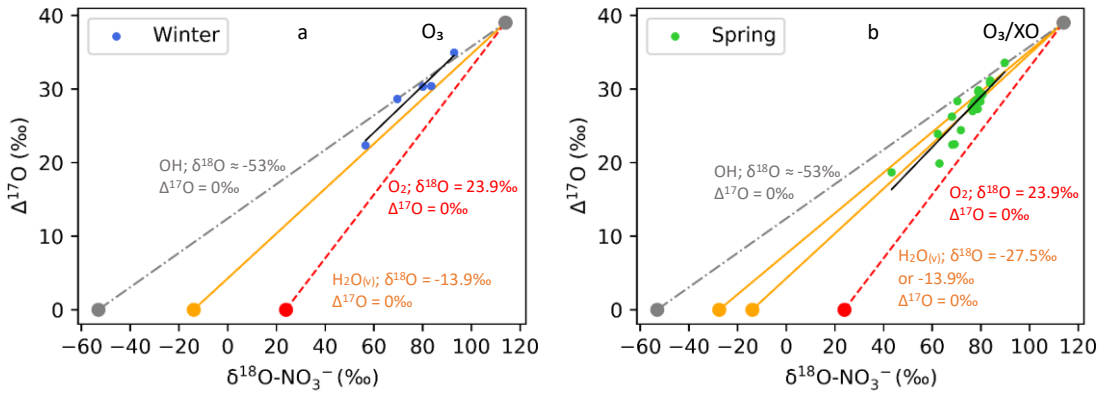


Figure 5. Winter and spring $\delta^{18}\text{O}\text{-NO}_3^-$ vs. $\Delta^{17}\text{O}\text{-NO}_3^-$ are plotted in panels (a) and (b), respectively. A straight line (black) is fitted to the data in each panel. In both panels the grey line represents the OH/ O_3 mixing line, the orange line represents the $\text{H}_2\text{O}_{(\text{v})}/\text{O}_3$ mixing line and the red line represents the O_2/O_3 mixing line. In panel b, an additional $\text{H}_2\text{O}_{(\text{v})}/\text{O}_3$ mixing line is included (also in orange) to account for potentially lower values of $\delta^{18}\text{O}\text{-H}_2\text{O}_{(\text{v})}$ ($\sim -27.5\text{‰}$) at 60° to 70° S.

Figure 6. Winter and spring $\delta^{18}\text{O}\text{-NO}_3^-$ vs. $\Delta^{17}\text{O}\text{-NO}_3^-$ are plotted in panels (a) and (b), respectively. A straight line (black) is fitted to the data in each panel. In both panels the grey line represents the OH/ O_3 mixing line, the orange line represents the $\text{H}_2\text{O}_{(\text{v})}/\text{O}_3$ mixing line and the red line represents the O_2/O_3 mixing line.

By contrast, observations made in spring are best represented by mixing between 3 major oxidants: $\text{H}_2\text{O}_{(\text{v})}$, O_3 and O_2 . The x-intercept in spring is $\sim -4\text{‰}$, making it more difficult to identify one low $\delta^{18}\text{O}$ end member. The oxidant source with the closest oxygen isotope composition is again $\text{H}_2\text{O}_{(\text{v})}$, indicating the prevalence of the OH pathway (when $\delta^{18}\text{O}\text{-OH} \sim \delta^{18}\text{O}\text{-H}_2\text{O}_{(\text{v})}$), however the x-intercept is greater in spring compared to winter, suggesting that the lower end member has a higher $\delta^{18}\text{O}$. $\text{H}_2\text{O}_{(\text{v})}$ data from the region suggest that we would not expect to see a $\delta^{18}\text{O} > -10\text{‰}$, therefore an increase in $\text{H}_2\text{O}_{(\text{v})}$ $\delta^{18}\text{O}$ from winter to spring can be ruled out. A more likely explanation is that the springtime lower endmember consists of some combination of $\text{H}_2\text{O}_{(\text{v})}$ and an additional higher $\delta^{18}\text{O}$ oxidant that is less abundant in winter. The higher $\delta^{18}\text{O}$ oxidant is likely atmospheric O_2 ($\delta^{18}\text{O} = 23.9\text{‰}$, $\Delta^{17}\text{O} = 0\text{‰}$ vs VSMOW; Barkan and Luz, 2005). This is consistent with the spread in the springtime observations, which are bound by the decreased $\text{H}_2\text{O}_{(\text{v})}/\text{O}_3$ mixing line to accommodate the influence of lower $\delta^{18}\text{O}\text{-H}_2\text{O}_{(\text{v})}$ at the high latitudes (Fig. 56b; orange line), and the atmospheric O_2/O_3 mixing line (Fig. 56b; red line).

The influence of atmospheric O_2 during spring likely results from the increased role for RO_2 (and/or HO_2) in NO_x cycling. This may be linked to increased RO_2 production over the mid-latitude Southern Ocean, derived from

Formatted: Font: (Default) Times New Roman, 10 pt

Formatted: Font: (Default) Times New Roman, 10 pt

Formatted: Justified, Tab stops: 3.13", Centered

Formatted: Font: (Default) Times New Roman, 10 pt

Formatted: Superscript

RONO₂ photolysis in the MBL (Burger et al., 2022). There is also evidence that sea ice can lead to enhanced peroxy radical production (Brough et al., 2019), resulting in the potential for increased RO₂ and HO₂ concentrations to be observed in air masses that traverse the sea ice zone before being sampled. δ¹⁸O-NO₃⁻ is greater in winter and spring compared to summer (Fig. 5), highlighting the increased control of O₃ on the oxygen isotopic composition of NO₃⁻ in winter and spring. Consistent with increased O₃ influence are seasonally resolved observations of O₃ concentration ([O₃]) at coastal Antarctica (Ishino et al., 2017; Shi et al, 2022) and Cape Grim, Tasmania (Derwent et al., 2016), the latter being more representative of the MBL. In all cases, maximum [O₃] are observed in winter, and minimum [O₃] are observed throughout summer. In spring, [O₃] concentrations are noticeably reduced compared to the winter, but slightly elevated compared to summer. [Higher δ¹⁸O-NO₃⁻ values in spring may also originate from NO_x oxidation by XO, for example BrO_x as discussed in Section 3.3.](#)

4 Conclusions

Seasonally resolved observations of atmospheric NO₃⁻ across the Atlantic Southern Ocean MBL suggest that natural NO_x sources dominate throughout the year. Similar NO₃⁻ sources are available to the MBL in both spring and summer, highlighting the importance of oceanic RONO₂ emissions in seasons other than the more frequently sampled summer months in the Southern Ocean. Although further research is required to improve our mechanistic and isotopic understanding of oceanic RONO₂ formation, fluxes and conversion to aerosol NO₃⁻, this work contributes to our growing understanding of how the surface ocean influences the atmospheric reactive N cycle and oxidation chemistry of the MBL (Altieri et al., 2021; Burger et al., 2022; Joyce et al., 2022).

Furthermore, the large sea ice extent characteristic of spring highlights the importance of snow-covered sea ice as a NO_x source, in addition to the well documented summer source from snow covered continental ice (Jones et al., 2001; Walters et al., 2019; Winton et al., 2020). [Currently no measurements of δ¹⁵N-NO₃⁻ from snowpack on sea ice exist for Antarctica, which is an important measurement gap that should be addressed in future studies.](#) The presence of sea ice may also play a role in the formation of peroxy radicals through its influence on chlorine chemistry when sunlight is available (Brough et al., 2019). Peroxy radicals (RO₂), H₂O_(v) and O₃ serve as the dominant atmospheric oxidants during spring, responsible for aerosol NO₃⁻ formation. In contrast, a lack of sunlight and sea ice influence is experienced during winter, and mixing between two end-members, H₂O_(v) and O₃, best explain the oxygen isotopic composition of the NO₃⁻ that is formed. Similar to coastal Antarctic sites, reduced daylight hours and/or increased O₃ abundance in the winter and spring MBL lead to greater O₃ influence on NO₃⁻ formation, compared to the summer when OH oxidation chemistry dominates.

Winter is characterised by very low [NO₃⁻] concentrations with δ¹⁵N signatures that reflect background conditions similar to that of the low latitude Atlantic Ocean (Morin et al., 2009). Interestingly, despite being collected off the coast of South Africa, the N and O isotopic composition of NO₃⁻ measured for the first wintertime sample reflects a stratospheric NO₃⁻ source signal. This is also supported by AMBTs that originate near Antarctica, where stratospheric denitrification is reported to occur (Savarino et al., 2007).

Our observations highlight the [potential power of N and O isotopes of nitrate in distinguishing between the various natural NO_x sources that result in NO₃⁻ formation, and constraining formation pathways of aerosol NO₃⁻.](#) In order

to improve the utility of the N and O isotopes in the polar atmosphere, more measurements of the isotopic composition of the regional sources, e.g., snow on sea ice, and regional processes, e.g., OH from HONO and sea ice oxidant emissions, is needed. Even though it is complex, the utility of the N isotopes in distinguishing between the various natural NO_x sources that result in NO₃⁻ formation in the MBL of the Atlantic Southern Ocean, especially in the less frequently sampled seasons of winter and spring is evident. Furthermore, the O isotopes serve as a useful tool for constraining formation pathways of aerosol NO₃⁻ seasonally. This is especially important in the Atlantic Southern Ocean where oxidation chemistry is poorly constrained (Beygi et al., 2011). The contribution of sea ice to oxidant production when sunlight returns in spring is also highlighted by the O isotopes. As such, these data may be useful to modelling efforts attempting to characterise N cycling between the surface ocean and lower atmosphere, and may help improve atmospheric oxidant budgets that are less understood in unpolluted low-NO_x environments.

Author contributions. KEA designed the study and sampling campaign, acquired funding and supervised the research. KEA and MGH provided financial and laboratory resources and assisted in data validation. EJ performed laboratory analysis of samples at Brown University. KAMS and JMB conducted the sampling at sea and JMB performed laboratory analysis at the University of Cape Town. JMB analysed the data and prepared the manuscript with contributions from all co-authors. KEA, MGH and EJ assisted with reviewing and editing the manuscript.

Competing interests. One author is a member of the editorial board of journal ACP. The authors declare no other conflicts of interest.

Data availability. Datasets for this research are available at <https://doi.org/10.5281/zenodo.7142722>

Acknowledgements. We thank the Captain and crew of the R/V *SA Agulhas II* for their support at sea and the Marine Biogeochemistry Laboratory in the Oceanography Department at the University of Cape Town for their assistance in the field and in the Laboratory. We thank Ruby Ho for analytical support. We thank Riesna Audh, Raquel Flynn, Shantelle Smith, Eleonora Puccinelli, Sina Wallschuss, Eesaa Harris and Sive Xokashe for nitrite concentration measurements and Sarah Fawcett and Raquel Flynn for quality controlling the nitrite concentration data. We thank the South African Weather Service (SAWS) for atmospheric temperature, sea level pressure and relative humidity data during all three voyages. This project has received funding from the European Union's Horizon 2020 research and innovation programme under grant agreement No 101003826 via project CRiceS (Climate Relevant interactions and feedbacks: the key role of sea ice and Snow in the polar and global climate system).

Financial Support. This research has been supported by the South African National Research Foundation through a Competitive Support for Rated Researchers Grant to KEA (111716) and a South African National Antarctic Programme Postgraduate Fellowship to JMB and Grant to KEA (110732). This research was further supported by the University of Cape Town through a University Research Council Launching Grant and VC Future Leaders 2030 Grant awarded to KEA. Additional support was provided by the National Research Foundation through a doctoral scholarship to JMB (138813) as well as by the European Union's Horizon 2020 research and innovation programme (Grant agreement No 101003826) via project CRiceS. This work was partially supported by the NSF (Award Number: 1851343) via the North Pacific Atmosphere project grant awarded to MGH.

References

Alexander, B., Sherwen, T., Holmes, C. D., Fisher, J. A., Chen, Q., Evans, M. J., and Kasibhatla, P.: Global inorganic nitrate production mechanisms: comparison of a global model with nitrate isotope observations, *Atmos. Chem. Phys.*, 20, 3859–3877, <https://doi.org/10.5194/acp-20-3859-2020>, 2020.

Altieri, K. E., Hastings, M. G., Gobel, A. R., Peters, A. J., and Sigman, D. M.: Isotopic composition of rainwater nitrate at Bermuda: the influence of air mass source and chemistry in the marine boundary layer, *J. Geophys. Res.-Atmos.*, 118, 11304–11316, <https://doi.org/10.1002/jgrd.50829>, 2013.

Altieri, K. E., Fawcett, S. E., and Hastings, M. G.: Reactive Nitrogen Cycling in the Atmosphere and Ocean, *Annu. Rev. Earth Pl. Sc.*, 49, 513–540, <https://doi.org/10.1146/annurev-earth-083120-052147>, 2021.

Baker, A.R., Weston, K., Kelly, S. D., Voss, M., Streu, P., and Cape, J. N.: Dry and wet deposition of nutrients from the tropical Atlantic atmosphere: links to primary productivity and nitrogen fixation, *Deep Sea Res. Part I Oceanogr. Res. Pap.*, 54(10), 1704–1720, <https://doi.org/10.1016/j.dsr.2007.07.001>, 2007.

Barkan, E., and Luz, B.: High precision measurements of $^{17}\text{O}/^{16}\text{O}$ and $^{18}\text{O}/^{16}\text{O}$ ratios in H_2O , *Rapid Commun. Mass Spectrom.*, 19, 3737–3742, <https://doi.org/10.1002/rcm.2250>, 2005.

Bauguitte, S. J.-B., Bloss, W. J., Evans, M. J., Salmon, R. A., Anderson, P. S., Jones, A. E., Lee, J. D., Saiz-Lopez, A., Roscoe, H. K., Wolff, E. W., and Plane, J. M. C.: Summertime NO_x measurements during the CHABLIS campaign: can source and sink estimates unravel observed diurnal cycles?, *Atmos. Chem. Phys.*, 12, 989–1002, <https://doi.org/10.5194/acp-12-989-2012>, 2012.

Berhanu, T. A., Meusinger, C., Erbland, J., Jost, R., Bhattacharya, S. K., Johnson, M. S., and Savarino, J.: Laboratory study of nitrate photolysis in Antarctic snow. II. Isotopic effects and wavelength dependence, *J. Chem. Phys.*, 140, 244306, <https://doi.org/10.1063/1.4882899>, 2014.

Berhanu, T. A., Savarino, J., Bhattacharya, S. K., and Vicars, W. C.: ^{17}O excess transfer during the $\text{NO}_2 + \text{O}_3 \rightarrow \text{NO}_3 + \text{O}_2$ reaction, *J. Chem. Phys.*, 136, 1–9, <https://doi.org/10.1063/1.3666852>, 2012.

Berhanu, T. A., Savarino, J., Erbland, J., Vicars, W. C., Preunkert, S., Martins, J. F., and Johnson, M. S.: Isotopic effects of nitrate photochemistry in snow: a field study at Dome C, Antarctica, *Atmos. Chem. Phys.*, 15, 11243–11256, <https://doi.org/10.5194/acp-15-11243-2015>, 2015.

Beygi, Z. H., Fischer, H., Harder, H. D., Martinez, M., Sander, R., Williams, J., Brookes, D. M., Monks, P. S., and Lelieveld, J.: Oxidation photochemistry in the Southern Atlantic boundary layer: unexpected deviations of photochemical steady state, *Atmos. Chem. Phys.*, 11, 8497–8513, <https://doi.org/10.5194/acp-11-8497-2011>, 2011.

Böhlke, J. K., Mroczkowski, S. J., and Coplen, T. B.: Oxygen isotopes in nitrate: new reference materials for $^{18}\text{O}:^{17}\text{O}:^{16}\text{O}$ measurements and observations on nitrate–water equilibrium, *Rapid Commun. Mass Sp.*, 17, 1835–1846, <https://doi.org/10.1002/rcm.1123>, 2003.

Brough, N., Jones, A. E., and Griffiths, P. T.: Influence of sea ice derived halogens on atmospheric HOx as observed in Springtime coastal Antarctica, *Geophys. Res. Lett.*, 46, 10168–10176, <https://doi.org/10.1029/2019GL083825>, 2019.

Burger, J. M., Granger, J., Joyce, E., Hastings, M. G., Spence, K. A. M., and Altieri, K. E.: The importance of alkyl nitrates and sea ice emissions to atmospheric NOx sources and cycling in the summertime Southern Ocean marine boundary layer, *Atmos. Chem. Phys.*, 22, 1081–1096, <https://doi.org/10.5194/acp-22-1081-2022>, 2022.

Formatted: Indent: Left: 0", First line: 0"

698 Casciotti, K. L., Sigman, D. M., Hastings, M. G., Böhlke, J. K., and Hilkert, A.: Measurement of the oxygen
 699 isotopic composition of nitrate in seawater and freshwater using the denitrifier method, *Anal. Chem.*, 74,
 700 4905–4912, <https://doi.org/10.1021/ac020113w>, 2002.
 701 Dahl, E. E. and Saltzman, S. E.: Alkyl nitrate photochemical production rates in North Pacific seawater, *Mar.*
 702 *Chem.*, 112, 137–141, <https://doi.org/10.1016/j.marchem.2008.10.002>, 2008.
 703 Dahl, E. E., Heiss, E. M., and Murawski, K.: The effects of dissolved organic matter on alkyl nitrate production
 704 during GOMECC and laboratory studies, *Mar. Chem.*, 142, 11–17,
 705 <https://doi.org/10.1016/j.marchem.2012.08.001>, 2012.
 706 Dar, S. S., Ghosh, P., Swaraj, A., and Kumar, A.: Graig-Gordon model validation using observed meteorological
 707 parameters and measured stable isotope ratios in water vapor over the Southern Ocean, *Atmos. Chem.*
 708 *Phys.*, 20, 11435–11449, <https://doi.org/10.5194/acp-20-11435-2020>, 2020.
 709 Davidson, E. A. and Kinglerlee, W.: A global inventory of nitric oxide emissions from soils, *Nutr. Cycl.*
 710 *Agroecosys.*, 48, 37–50, <https://doi.org/10.1023/A:1009738715891>, 1997.
 711 Derwent, R. G., Parrish, D. D., Galbally, I. E., Stevenson, D. S., Doherty, R. M., Young, P. J., and Shallcross, D.
 712 E.: Interhemispheric differences in seasonal cycles of tropospheric ozone in the marine boundary layer:
 713 Observation-model comparisons, *J. Geophys. Res. Atmos.*, 121, 11075–11085,
 714 <https://doi.org/10.1002/2016JD024836>, 2016.
 715 Elliott, E. M., Kendall, C., Wankel, S. D., Burns, S. A., Boyer, E. W., Harlin, K., Bain, D. J., and Butler, T. J.:
 716 Nitrogen isotopes as indicators of NO_x source contributions to atmospheric nitrate deposition across the
 717 Midwestern and Northeastern United States, *Environ. Sci. Technol.*, 41, 7661–7667,
 718 <https://doi.org/10.1021/es070898t>, 2007.
 719 Elliot, E. M., Yu, Z., Cole, A. S., and Coughlin, J. G.: Isotopic advances in understanding reactive nitrogen
 720 deposition and atmospheric processing, *Sci. Total Environ.*, 662, 393–403,
 721 <https://doi.org/10.1016/j.scitotenv.2018.12.177>, 2019.
 722 [Erbland, J., Vickers, W. C., Savarino, J., Morin, S., Frey, M. M., Frosini, D., Vince, E., and Martins, J. M. F.: Air-](#)
 723 [snow transfer of nitrate on the East Antarctic Plateau – Part 1: Isotopic evidence for a photolytically](#)
 724 [driven dynamic equilibrium in summer, *Atmos. Chem. Phys.*, 13, 6403–6419,](#)
 725 <https://doi.org/10.5194/acp-13-6403-2013>, 2013.
 726
 727 Fang, Y. T., Koba, K., Wang, X. M., Wen, D. Z., Li, J., Takebayashi, Y., Liu, X. Y., and Yoh, M.: Anthropogenic
 728 imprints on nitrogen and oxygen isotopic composition of precipitation nitrate in a nitrogen-polluted city
 729 in southern China, *Atmos. Chem. Phys.*, 11, 1313–1325, <https://doi.org/10.5194/acp-11-1313-2011>,
 730 2011.
 731 [Fibiger, D. L., and Hastings, M. G.: First Measurements of the Nitrogen Isotopic](#)
 732 [Composition of NO_x from Biomass Burning, *Environ. Sci. Technol.*, 50, 21, 11569–11574,](#)
 733 <https://doi.org/10.1021/acs.est.6b03510>, 2016.
 734 Fibiger, D. L., Hastings, M. G., Dibb, J. E., and Huey, L. G.: The preservation of atmospheric nitrate in snow at
 735 Summit, Greenland, *Geophys. Res. Lett.*, 40, 3484–3489, <https://doi.org/10.1002/grl.50659>, 2013.
 736 Finlayson-Pitts, B. J. and Pitts, J. N.: Chemistry of the upper and lower troposphere, Academic Press, San Diego,
 737 California, <https://doi.org/10.1016/B978-0-12-257060-5.X5000-X>, 2000.

Formatted: Subscript

Formatted: Indent: Hanging: 0.01"

738 Fisher, J. A., Atlas, E. L., Barletta, B., Meinardi, S., Blake, D. R., Thompson, C. R., Ryerson, T. B., Peischl, J.,
 739 Tzompa-Sosa, Z. A., and Murray, L. T.: Methyl, ethyl and propyl nitrates: global distribution and impacts
 740 on reactive nitrogen in remote marine environments, *J. Geophys. Res.-Atmos.*, 123, 12412–12429,
 741 <https://doi.org/10.1029/2018JD029046>, 2018.
 742 Frey, M. M., Savarino, J., Morin, S., Erbland, J., and Martins, J. M. F.: Photolysis imprint in the nitrate stable
 743 isotope signal in snow and atmosphere of East Antarctica and implications for reactive nitrogen cycling,
 744 *Atmos. Chem. Phys.*, 9, 8681–8696, <https://doi.org/10.5194/acp-9-8681-2009>, 2009.
 745 [Grannas, A. M., Jones, A. E., Dibb, J., Ammann, M., Anastasio, C., Beine, H. J., Bergin, M., Bottenheim, J.,](#)
 746 [Boxe, C. S., Carver, G., Chen, G., Crawford, J. H., Dominé, F., Frey, M. M., Guzmán, M. I., Heard, D.](#)
 747 [E., Helmig, D., Hoffmann, M. R., Honrath, R. E., Huey, L. G., Hutterli, M., Jacobi, H. W., Klán, P.,](#)
 748 [Lefer, B., McConnell, J., Plane, J., Sander, R., Savarino, J., Shepson, P. B., Simpson, W. R., Sodeau, J.](#)
 749 [R., von Glasow, R., Weller, R., Wolff, E. W., and Zhu, T.: An overview of snow photochemistry:](#)
 750 [evidence, mechanisms and impacts, *Atmos. Chem. Phys.*, 7, 4329–4373, \[https://doi.org/10.5194/acp-7-\]\(https://doi.org/10.5194/acp-7-4329-2007\)](#)
 751 [4329-2007, 2007.](#)
 752 Grasshoff, K., Kremling, K., and Ehrhardt, M.: *Methods of seawater analysis*, Verlag Chemi, Florida, 1983.
 753
 754 Hamilton, D. S., Lee, L. A., Pringle, K. J., Reddington, C. L., Spracklen, D. V., and Carslaw, K. S.: Occurrence
 755 of pristine aerosol environments on a polluted planet, *P. Natl. Acad. Sci. USA*, 111, 18466–18471,
 756 <https://doi.org/10.1073/pnas.1415440111>, 2014.
 757 Hastings, M. G., Sigman, D. M., and Lipschultz, F.: Isotopic evidence for source changes of nitrate in rain at
 758 Bermuda, *J. Geophys. Res.*, 108, 4790, <https://doi.org/10.1029/2003JD003789>, 2003.
 759 Haywood, J. and Boucher, O.: Estimates of the direct and indirect radiative forcing due to tropospheric aerosols:
 760 a review, *Rev. Geophys.*, 38, 513–543, <https://doi.org/10.1029/1999RG000078>, 2000.
 761 [Heidenreich, J. E. III., and Thiemens, M. H.: A non-mass-dependent oxygen isotope effect in](#)
 762 [the production of ozone from molecular oxygen: the role of symmetry in isotope chemistry, *J. Chem.*](#)
 763 [Phys.](#), 84, 2129–2136, <https://doi.org/10.1063/1.450373>, 1986.
 764 Hoering, T.: The isotopic composition of the ammonia and the nitrate ion in rain, *Geochim. Cosmochim. Ac.*, 12,
 765 97–102, [https://doi.org/10.1016/0016-7037\(57\)90021-2](https://doi.org/10.1016/0016-7037(57)90021-2), 1957.
 766 IPCC: Boucher, O. D., Randall, P., Artaxo, C., Bretherton, G., Feingold, P., Forster, V.-M., Kerminen, Y., Kondo,
 767 H., Liao, U., Lohmann, P., Rasch, S.K., Satheesh, S., Sherwood, B., Stevens, and Zhang, X. Y.: Clouds
 768 and Aerosols, in: *Climate Change 2013: The Physical Science Basis. Contribution of Working Group I*
 769 *to the Fifth Assessment Report of the Intergovernmental Panel on Climate Change*, edited by: Stocker,
 770 T. F., Qin, D., Plattner, G.-K., Tignor, M., Allen, S. K., Boschung, J., Nauels, A., Xia, Y., Bex, V., and
 771 Midgley, P. M., Cambridge University Press, Cambridge, United Kingdom and New York, NY, USA,
 772 2013.
 773 Ireland, T. R., Avila, J., Greenwood, R. C., Hicks, L. J., and Bridges, J. C.: Oxygen Isotopes and Sampling of the
 774 Solar System, *Space Sci. Rev.*, 216(25), 1–60, <https://doi.org/10.1007/s11214-020-0645-3>, 2020.
 775 Ishino, S., Hattori, S., Savarino, J., Jourdain, B., Preunkert, S., Legrand, M., Caillon, N., Barbero, A., Kuribayashi,
 776 K., and Yoshida, N.: Seasonal variations of triple oxygen isotopic compositions of atmospheric sulfate,

Formatted: Font: Not Italic

Formatted: Indent: Hanging: 0.01"

Formatted: Font: Not Italic

nitrate, and ozone at Dumont d'Urville, coastal Antarctica, *Atmos. Chem. Phys.*, 17, 3713–3727
<https://doi.org/10.5194/acp-17-3713-2017>, 2017.

Jacobi, H.-W., Weller, R., Jones, A. E., Anderson, P. S., & Schrems, O.: Peroxyacetyl nitrate (PAN) concentrations in the Antarctic troposphere measured during the photochemical experiment at Neumayer (PEAN'99), *Atmos. Environ.*, 34, 5235–5247, [https://doi.org/10.1016/S1352-2310\(00\)00190-4](https://doi.org/10.1016/S1352-2310(00)00190-4), 2000.

Jones, A. E., Weller, R., Wolff, E. W., and Jacobi, H.-W.: Speciation and rate of photochemical NO and NO₂ production in Antarctic snow, *Geophys. Res. Lett.*, 27, 345–348, <https://doi.org/10.1029/1999GL010885>, 2000.

Jones, A. E., Weller, R., Anderson, P. S., Jacobi, H.-W., Wolff, E. W., Schrems, O., and Miller, H.: Measurements of NO_x emissions from the Antarctic snowpack, *Geophys. Res. Lett.*, 28, 1499–1502, <https://doi.org/10.1029/2000GL011956>, 2001.

Joyce, E. E., Balint, S. J., and Hastings, M. G.: Isotopic evidence that alkyl nitrates are important to aerosol nitrate formation in the equatorial Pacific, *Geophys. Res. Lett.*, 49(16), 1–10, <https://doi.org/10.1029/2022GL099960>, 2022.

Kaiser, J., Hastings, M. G., Houlton, B. Z., Rockmann, T., and Sigman, D. M.: Triple Oxygen Isotope Analysis of Nitrate Using the Denitrifier Method and Thermal Decomposition of N₂O, *Anal. Chem.*, 79, 599–607, <https://doi.org/10.1021/ac061022s>, 2007.

Kamezaki, K., Hattori, S., Iwamoto, Y., Ishino, S., Furutani, H., Miki, Y., Uematsu, M., Miura, K., and Yoshida, N.: Tracing the sources and formation pathways of atmospheric particulate nitrate over the Pacific Ocean using stable isotopes, *Atmos. Environ.*, 209, 152–166, <https://doi.org/10.1016/j.atmosenv.2019.04.026>, 2019.

Kasibhatla, P., Sherwen, T., Evans, M. J., Carpenter, L. J., Reed, C., Alexander, B., Chen, Q., Sulprizio, M. P., Lee, J. D., Read, K. A., Bloss, W., Crilley, L. R., Keene, W. C., Pszenny, A. A. P., and Hodzic, A.: Global impact of nitrate photolysis in sea-salt aerosol on NO_x, OH, and O₃ in the marine boundary layer, *Atmos. Chem. Phys.*, 18, 11185–11203, <https://doi.org/10.5194/acp-18-11185-2018>, 2018.

Lakkala, K., Aun, M., Sanchez, R., Bernhard, G., Asmi, E., Meinander, O., Nollas, F., Hülsen, G., Karppinen, T., Aaltonen, V., Arola, A., and de Leeuw, G.: New continuous total ozone, UV, VIS and PAR measurements at Marambio, 64°S, Antarctica, *Earth Syst. Sci. Data*, 12, 947–960, <https://doi.org/10.5194/essd-12-947-2020>, 2020.

Lawrence, M. G., and Crutzen, P. J.: Influence of NO_x emissions from ships on tropospheric photochemistry and climate, *Nature*, 402, 167–170, <https://doi.org/10.1038/46013>, 1999.

Lee, H.-M., Henze, D. K., Alexander, B., and Murray, L. T.: Investigating the sensitivity of surface-level nitrate seasonality in Antarctica to primary sources using a global model, *Atmos. Environ.*, 89, 757–767, <https://doi.org/10.1016/j.atmosenv.2014.03.003>, 2014.

[Legrand, M., Preunkert, S., Frey, M., Bartels-Rausch, Th., Kukui, A., King, M. D., Savarino, J., Kerbrat, M., and Jourdain, B.: Large mixing ratios of atmospheric nitrous acid \(HONO\) at Concordia \(East Antarctic Plateau\) in summer: a strong source from surface snow?, *Atmos. Chem. Phys.*, 14, 9963–9976, <https://doi.org/10.5194/acp-14-9963-2014>, 2014.](#)

816 Li, J., Davy, P., Harvey, M., Katzman, T., Mitchell, T., and Michalski, G.: Nitrogen isotopes in nitrate aerosols
 817 collected in the remote marine boundary layer: Implications for nitrogen isotopic fractionations among
 818 atmospheric reactive nitrogen species, *Atmos. Environ.*, 245, 1-10,
 819 <https://doi.org/10.1016/j.atmosenv.2020.118028>, 2021.
 820 Li, C., Chen, J., Angot, H., Zheng, W., Shi, G., Ding, M., Du, Z., Zhang, Q., Ma, X., Kang, S., Xiao, C., Ren, J.,
 821 and Qin, D.: Seasonal Variation of Mercury and its Isotopes in Atmospheric Particles at the Coastal
 822 Zhongshan Station, Eastern Antarctica, *Environ. Sci. Technol.*, 54, 11344-11355,
 823 <https://dx.doi.org/10.1021/acs.est.0c04462>, 2020.
 824 McCabe, J. R., Thiemens, M. H., Savarino, J.: A record of ozone variability in South Pole Antarctic snow: Role
 825 of nitrate oxygen isotopes, *J. Geophys. Res.*, 112, D12303, <https://doi.org/10.1029/2006JD007822>, 2007.
 826 Michalski, G., Scott, Z., Kabilig, M., and Thiemens, M. H.: First measurements and modeling of $\Delta^{17}\text{O}$ in
 827 atmospheric nitrate, *Geophys. Res. Lett.*, 30, 1870, <https://doi.org/10.1029/2003GL017015>, 2003.
 828 Michalski, G., and Bhattacharya, S. K.: The role of symmetry in the mass independent isotope effect in ozone,
 829 *PNAS*, 106(14), 5493-5496, <http://www.jstor.org/stable/40454817>, 2009.
 830 Michalski, G., Bhattacharya, S. K., and Mase, D. F.: Oxygen isotope dynamics of atmospheric nitrate and its
 831 precursor molecules, in: *Handbook of environmental isotope geochemistry. Advances in Isotope*
 832 *Geochemistry*, edited by: Baskaran, M., Springer, Berlin, Heidelberg, 613-635,
 833 https://doi.org/10.1007/978-3-642-10637-8_30, 2012.
 834 [Miller, D. J., Chai, J., Guo, F., Dell, C. J., Karsten, H., and Hastings, M. G: Isotopic Composition of In Situ Soil](#)
 835 [\$\text{NO}_x\$ Emissions in Manure-Fertilized Cropland, *Geophys. Res. Lett.*, 45, 21, 12058-12066,
 836 \[<https://doi.org/10.1029/2018GL079619>, 2018.\]\(#\)
 837 \[Morin, S., Erbland, J., Savarino, J., Domine, F., Bock, J., Friess, U., Jacobi, H.-W., Sihler, H., and Martins, J. M.\]\(#\)
 838 \[F.: An isotopic view on the connection between photolytic emissions of \\$\text{NO}_x\\$ from the Arctic snowpack\]\(#\)
 839 \[and its oxidation by reactive halogens, *J. Geophys. Res.*, 117, D14,
 840 \\[<https://doi.org/10.1029/2011JD016618>, 2012.\\]\\(#\\)
 841
 842 Morin, S., Savarino, J., Frey, M. M., Domine, F., Jacobi, H. W., Kaleschke, L., and Martins, J. M.: Comprehensive
 843 isotopic composition of atmospheric nitrate in the Atlantic Ocean boundary layer from 65° S to 79° N,
 844 *J. Geophys. Res.*, 114, D05303, <https://doi.org/10.1029/2008JD010696>, 2009.
 845 Morin, S., Sander, R., Savarino, J.: Simulation of the diurnal variations of the oxygen isotope anomaly \\(\\$\Delta^{17}\text{O}\\$ \\) of
 846 reactive atmospheric species, *Atmos. Chem. Phys.*, 11, 3653-3671, \\[https://doi.org/10.5194/acp-11-3653-\\]\\(https://doi.org/10.5194/acp-11-3653-2011\\)
 847 2011, 2011.
 848 Nesbitt, S. W., Zhang, R., and Orville, R. E.: Seasonal and global \\$\text{NO}_x\\$ production by lightning estimated from
 849 the Optical Transient Detector \\(OTD\\), *Tellus B*, 52, 1206-1215,
 850 <https://doi.org/10.3402/tellusb.v52i5.17098>, 2000.
 851 Obbard, R. W.: Microplastics in Polar Regions: The role of long range transport, *Curr. Opin. in Environ. Sci.*, 1,
 852 24-29, <https://doi.org/10.1016/j.coesh.2017.10.004>, 2018.
 853 Park, S. S. and Kim, Y. J.: Source contributions to fine particulate matter in an urban atmosphere, *Chemosphere*,
 854 59, 217-226, <https://doi.org/10.1016/j.chemosphere.2004.11.001>, 2005.\]\(#\)](#)

Formatted: Subscript

Formatted: Font: Not Italic

Formatted: Font: Not Italic

Formatted: Font: Not Italic

Formatted: Font: Not Bold

855 Paton-Walsh, C., Emmerson, K. M., Garland, R. M., Keywood, M., Hoelzemann, J. J., Huneeus, N., Buchholz,
856 R. R., Humphries, R. S., Altieri, K., Schmale, J., Wilson, S. R., Labuschagne, C., Kalisa, E., Fisher, J.
857 A., Deutscher, N. M., van Zyl, P. G., Beukes, J. P., Joubert, W., Martin, L., Mkololo, T., Barbosa, C.,
858 Anrade, M. de F., Schofield, R., Mallet, M. D., Harvey, M. J., Formenti, P., Piketh, S. J., and Olivares,
859 G.: Key challenges for tropospheric chemistry in the Southern Hemisphere, *Elem. Sci. Anth.*, 10(1), 1-
860 35, <https://doi.org/10.1525/elementa.2021.00050>, 2022.

861 Reed, C., Evans, M. J., Crilley, L. R., Bloss, W. J., Sherwen, T., Read, K. A., Lee, J. D., and Carpenter, L. J.:
862 Evidence for renoxification in the tropical marine boundary layer, *Atmos. Chem. Phys.*, 17, 4081-4092,
863 <https://doi.org/10.5194/acp-17-4081-2017>, 2017.

864 Rolph, G. D.: Real-time Environmental Applications and Display System (READY) Website, NOAA Air
865 Resources Laboratory, College Park, MD, available at: <https://www.ready.noaa.gov/index.php> (last
866 access: June 2022), 2016.

867 Romer, P. S., Wooldridge, P. J., Crounse, J. D., Kim, M. J., Wennberg, P. O., Dibb, J. E., Scheuer, E., Blake, D.
868 R., Meinardi, S., Brosius, A. L., Thames, A. B., Miller, D. O., Brune, W. H., Hall, S. R., Ryerson, T. B.,
869 and Cohen, R. C.: Constraints on Aerosol Nitrate Photolysis as a Potential Source of HONO and NO_x,
870 *Environ. Sci. Technol.*, 52, 13738-13746, <https://doi.org/10.1021/acs.est.8b03861>, 2018.

871 Savarino, J., Kaiser, J., Morin, S., Sigman, D. M., and Thiemens, M. H.: Nitrogen and oxygen isotopic constraints
872 on the origin of atmospheric nitrate in coastal Antarctica, *Atmos. Chem. Phys.*, 7, 1925-1945,
873 <https://doi.org/10.5194/acp-7-1925-2007>, 2007.

874 [Savarino, J., Bhattacharya, S. K., Morin, S., Baroni, M., and Doussin, J.-F.: The NO+O₃ Reaction: A Triple](#)
875 [Oxygen Isotope Perspective on the Reaction Dynamics and Atmospheric Implications for the Transfer](#)
876 [of the Ozone Isotope Anomaly, *J. Chem. Phys.*, 128, 19, 194303, <https://doi.org/10.1063/1.2917581>,](#)
877 [2008.](#)

878 Savarino, J., Vicars, W. C., Legrand, M., Preunkert, S., Jourdain, B., Frey, M. M., Kukui, A., Caillon, N., and
879 Roca, J. G.: Oxygen isotope mass balance of atmospheric nitrate at Dome C, East Antarctica, during the
880 OPALE campaign, *Atmos. Chem. Phys.*, 16, 2659-2673, <https://doi.org/10.5194/acp-16-2659-2016>,
881 2016.

882 Schmale, J., Baccarini, A., Thurnherr, I., Henning, S., Efraim, A., Regayre, L., Bolas, C., Hartmann, M., Welti,
883 A., Lehtipalo, K., Aemisegger, F., Tatzelt, C., Landwehr, S., Modini, R. L., Tummon, F., Johnson, J. S.,
884 Harris, N., Schnaiter, M., Toffoli, A., Derkani, M., Bukowiecki, N., Stratmann, F., Dommen, J.,
885 Baltensperger, U., Wernli, H., Rosenfeld, D., Gysel-Beer, M., and Carslaw, K. S.: Overview of the
886 Antarctic Circumnavigation Expedition: study of preindustrial-like aerosols and their climate effects
887 (ACE-SPACE), *Bull. Am. Meteorol. Soc.*, 100(11), 2260-2283, 2019.

888 Schumann, U. and Huntrieser, H.: The global lightning-induced nitrogen oxides source, *Atmos. Chem. Phys.*, 7,
889 3823-3907, <https://doi.org/10.5194/acp-7-3823-2007>, 2007.

890 Shi, G., Buffen, A. M., Ma, H., Hu, Z., Sun, B., Li, C., Yu, J., Ma, T., An, C., Jiang, S., Li, Y., and Hastings, M.
891 G.: Distinguishing summertime atmospheric production of nitrate across the East Antarctic ice
892 sheet, *Geochim. Cosmochim. Ac.*, 231, 1-14, <https://doi.org/10.1016/j.gca.2018.03.025>, 2018.

893 Shi, G., Ma, H., Zhu, Z., Hu, A., Chen, Z., Jiang, Su., An, C., Yu, J., Ma, T., Li, Y., Sun, B., and Hastings, M. G.:
894 Using stable isotopes to distinguish atmospheric nitrate production and its contribution to the surface

Formatted: Subscript

Formatted: Font: Not Italic

Formatted: Font: Not Italic

ocean across hemispheres, *Earth & Planet. Sci. Lett.*, 564, 116914, <https://doi.org/10.1016/j.epsl.2021.116914>, 2021.

Shi, G., Li, C., Li, Y., Chen, Z., Ging, M., Ma, H., Jiang, S., An, C., Guo, J., Sun, B., and Hastings, M. Q.: Isotopic constraints on sources, production, and phase partitioning for nitrate in the atmosphere and snowfall in coastal East Antarctica, *Earth & Planet. Sci. Lett.*, 578, 1-12, <https://doi.org/10.1016/j.epsl.2021.117300>, 2022.

Sigman, D. M., Casciotti, K. L., Andreani, M., Barford, C., Galanter, M., and Böhlke, J. K.: A bacterial method for the nitrogen isotopic analysis of nitrate in seawater and freshwater, *Anal. Chem.*, 73, 4145–4153, <https://doi.org/10.1021/ac010088e>, 2001.

Stein, A. F., Draxler, R. R., Rolph, G. D., Stunder, B. J. B., Cohen, M. D., and Ngan, F.: NOAA's HYSPLIT atmospheric transport and dispersion modeling system, *B. Am. Meteorol. Soc.*, 96, 2059–2077, <https://doi.org/10.1175/BAMS-D-14-00110.1>, 2015.

Theimens, M. H., History and Applications of Mass-Independent Isotope Effects, *Annu. Rev. Earth Planet. Sci.*, 34, 217-262, <https://doi.org/10.1146/annurev.earth.34.031405.125026>, 2006.

van der A, R. J., Eskes, H. J., Boersma, K. F., van Noije, T. P., Van Roozendaal, M., De Smedt, I., Peters, D. H. M. U., and Meijer, E. W.: Trends, seasonal variability and dominant NO_x source derived from a ten year record of NO₂ measured from space, *J. Geophys. Res.*, 113, D04302, <https://doi.org/10.1029/2007JD009021>, 2008.

Vicars, W. C. and Savarino, J.: Quantitative constraints on the 17O-excess (17O) signature of surface ozone: Ambient measurements from 50° N to 50° S using the nitrite-coated filter technique, *Geochim. Cosmochim. Ac.*, 135, 270–287, <https://doi.org/10.1016/j.gca.2014.03.023>, 2014.

Von Savigny, C., Ulasi, E.P., Eichmann, K.-U., Bovensmann, H., and Burrows, J. P.: Detection and mapping of polar stratospheric clouds using limb scattering observations, *Atmos. Chem. Phys.*, 5, 3071-3079, <https://doi.org/10.5194/acp-5-3071-2005>, 2005.

Wagenbach, D., Legrand, M., Fischer, H., Pichlmayer, F., and Wolff, E.W.: Atmospheric near-surface nitrate at coastal Antarctic sites, *J. Geophys. Res.*, 103(D9), 11007-11020, <https://doi.org/10.1029/97JD03364>, 1998.

Walters, W. W. and Michalski, G.: Theoretical calculation of nitrogen isotope equilibrium exchange fractionation factors for various NO_y molecules, *Geochim. Cosmochim. Ac.*, 164, 284–297, <https://doi.org/10.1016/j.gca.2015.05.029>, 2015.

Walters, W. W., Simonini, D. S., and Michalski, G.: Nitrogen isotope exchange between NO and NO₂ and its implications for δ¹⁵N variations in tropospheric NO_x and atmospheric nitrate, *Geophys. Res. Lett.*, 43, 440–448, <https://doi.org/10.1002/2015GL066438>, 2016.

Walters, W. W., Michalski, G., Böhlke, J. K., Alexander, B., Savarino, J., and Thiemens, M. H.: Assessing the seasonal dynamic of nitrate and sulfate aerosols at the South Pole utilizing stable isotopes, *J. Geophys. Res.-Atmos.*, 124, 8161–8177, <https://doi.org/10.1029/2019JD030517>, 2019.

Wang, Z., Stephens, G., Deshler, T., Treppe, C., Parish, T., Vane, D., Winker, D., Liu, D., and Adhikari, L.: Association of Antarctic polar stratospheric cloud formation on tropospheric cloud systems, *Geophys. Res. Lett.*, 35, L13806, <https://doi.org/10.1029/2008GL034209>, 2008.

934 Winton, V. H. L., Ming, A., Caillon, N., Hauge, L., Jones, A. E., Savarino, J., Yang, X., and Frey, M. M.:
 935 Deposition, recycling, and archival of nitrate stable isotopes between the air-snow interface: comparison
 936 between Dronning Maud Land and Dome C, Antarctica, *Atmos. Chem. Phys.*, 20, 5861-5885,
 937 <https://doi.org/10.5194/acp-20-5861-2020>, 2020.
 938 Ye, C., Zhou, X., Pu, D., Stutz, J., Festa, J., Spolaor, M., Tsai, C., Cantrell, C., Mauldin III, R. L., Campos, T.,
 939 Weinheimer, A., Hornbrook, R. S., Apel, E. C., Guenther, A., Kaser, L., Yuan, B., Karl, T., Haggerty, J.,
 940 Hall, S., Ullmann, K., Smith, J. N., Ortega, J., and Christoph, K.: Rapid cycling of reactive nitrogen in
 941 the marine boundary layer, *Nature*, 532, 489-491, <https://doi.org/10.1038/nature17195>, 2016.
 942 Zhou, X., Gao, H., He, Y., Huang, G., Bertman, S. B., Civerolo, K., and Schwab, J.: Nitric acid photolysis on
 943 surfaces in low-NO_x environments: Significant atmospheric implications, *Geophys. Res. Lett.*, 23,
 944 2217, <https://doi.org/10.1029/2003GL018620>, 2003.
 945 Zong, Z., Wang, X., Tian, C., Chen, Y., Fang, Y., Zhang, F., Li, C., Sun, J., Li, J., and Zhang, G.: First assessment
 946 of NO_x sources at a regional background site in North China using isotopic analysis linked with
 947 modeling, *Environ. Sci. Technol.*, 51, 5923–5931, <https://doi.org/10.1021/acs.est.6b06316>, 2017.
 948